EURATOM

Project Deliverable

Project number:	Project Acronym:	Project title:
212246	SEDENTEXCT	Safety and Efficacy of a New and Emerging Dental X-ray Modality

Instrument:	Activity code:
Collaborative Project (Small or medium-scale focused research project)	**Fission-2007-3.2-01**

Start date of project:	Duration:
1 January 2008	**42 months**

Title:
D2.1: Definition of a standard index for characterizing the CBCT dose distribution

Contractual Delivery date:	Actual Delivery date:
Version 1.0: 30 June 2009 **Version 2.0: 30 September 2009*** *Owing to difficulties deriving the dose index, the EC Project Officer agreed that the deliverable be phased.	**Version 1.0: 25 June 2009** **Version 2.0: 30 September 2009** **Version 3.0: 12 March 2010** **Version 3.1: 16 March 2010**

Organisation name of lead beneficiary for this Deliverable:	Document version:
KULeuven (Katholieke Universiteit Leuven)	**v3.1**

Dissemination level:		
PU	Public	
PP	Restricted to other programme participants (including the Commission)	
RE	Restricted to a group defined by the consortium (including the Commission)	
CO	Confidential, only for members of the consortium (including the Commission)	**X**

Authors (organisations):

Ria Bogaerts (KUL): WP2 Lead
Ruben Pauwels (KUL)
Hilde Bosmans (KUL)
Anne Walker (UNIMAN)
Chrysoula Theodorakou (UNIMAN)

Abstract:
In this deliverable report, dose measurements from dental Cone Beam Computed Tomography (CBCT) devices are presented in cylindrical head size water and Poly (methyl methacrylate) (PMMA) phantoms and anthropomorphic (adult and child) phantoms, using thermoluminescent dosimeters (TLD), radiochromic films and a small-volume ion chamber.

It was found that the three-dimensional dose distribution can be asymmetrical for dental CBCT exposures throughout a homogeneous phantom, due to an asymmetrical positioning of the isocentre and/or partial rotation of the X-ray source.

Furthermore, the scatter tail along the z-axis was found to have a distinct shape, generally resulting in a significant drop in absorbed dose outside the primary beam.

Anthropomorphic phantom measurements showed large differences in absorbed organ doses and effective dose for different CBCT devices and protocols, depending on the Field of View (FOV) size and positioning, and exposure settings.

Based on the dose distribution measurements, a dose index was defined. The dose index contains information regarding the volumetric dose deposition can be measured routinely and is relevant to patient risk. Different possibilities are presented, as there is no optimal solution due to the complicated dose distribution, exposure geometry of CBCT and practical aspects of a quality control protocol. However, the proposed indices all provide an estimation of the dose which is deposited throughout a head-sized volume, and can be implemented into practice providing the appropriate equipment (phantom & dosimeter) are available.

Table of Contents

1 The Context

1.1 SEDENTEXCT aims and objectives

The aim of this project is the acquisition of the key information necessary for sound and scientifically based clinical use of dental Cone Beam Computed Tomography (CBCT). In order that safety and efficacy are assured and enhanced in the 'real world', the parallel aim is to use the information to develop evidence-based guidelines dealing with justification, optimisation and referral criteria and to provide a means of dissemination and training for users of CBCT. The objectives and methodology of the collaborative project are:

1. To develop evidence-based guidelines on use of CBCT in dentistry, including referral criteria, quality assurance guidelines and optimisation strategies. Guideline development will use systematic review and established methodology, involving stakeholder input.

2. To determine the level of patient dose in dental CBCT, paying special attention to paediatric dosimetry, and personnel dose.

3. To perform diagnostic accuracy studies for CBCT for key clinical applications in dentistry by use of in vitro and clinical studies.

4. To develop a quality assurance programme, including a tool/tools for quality assurance work (including a marketable quality assurance phantom) and to define exposure protocols for specific clinical applications.

5. To measure cost-effectiveness of important clinical uses of CBCT compared with traditional methods.

6. To conduct valorisation, including dissemination and training, activities via an 'open access' website.

At all points, stakeholder involvement will be intrinsic to study design.

1.2 Work package 2 (WP2) objectives

It is fundamental to radiation protection that the benefits of a procedure using ionizing radiation outweigh the risks; this is incorporated into the relevant European Directive 97/43/Euratom. The limited studies in the literature indicate that the radiation dose achievable with CBCT units is substantially less than conventional CT but higher than conventional dental imaging. In addition the radiation dose varies according to the particular manufacturer's system being assessed. For example, one system may give a dose ten times another for the same examination. Doses are many times greater than those for conventional 'dental' examinations. Dose depends upon the size of the volume of the patient imaged and the other selected technique factors.

These studies suffer because they are individually limited to reports related to one or two CBCT systems. More work is needed to verify this limited literature

on a greater range of current CBCT systems and without the inter-study variation in measurement methodologies; the research will achieve this. Importantly, however, our research will specifically deal with paediatric dosimetry, an area that has not been previously assessed using anatomically appropriate paediatric phantoms. Our research will also develop a robust system of Monte-Carlo dose simulation for CBCT that will facilitate optimisation of exposures.

The overall aim of this work package is to determine the level of (1) patient dose in dental CBCT, paying special attention to paediatric dosimetry, and (2) personnel dose. These goals correspond to the following sub-objectives:

1. To develop a method to readily characterise the dose distribution for different scanners, using measurements simply performed in the field, to allow simple conversion to effective dose.
2. To determine the scatter dose distribution around scanners and explore the consequences for operator dose.

1.3 Deliverable D2.1

Deliverable D2.1 (Definition of a standard index for characterizing the CBCT dose distribution) describes the development of a standard index of three-dimensional (volumetric) dose distribution, which can be routinely measured with common dosimetry methods in an inexpensive and simple phantom. The general goal of the project is to achieve an index which would parallel the use of Computed Tomography Dose Index (CTDI) used in axial, helical and multi-slice CT. The dose index would be used a) for quality control purposes to compare to manufacturers specifications, to confirm consistency of performance and to inter-compare different dental CBCT systems and b) with conversion factors to allow an estimate of patient risk (e.g. effective dose).

CTDI is a dose index that can estimate the multiple scan average dose for axial, helical and MSCT scanners in a standardised and convenient way. The radiation dose profile along the central axis (z-axis) of a homogenous cylindrical poly-methyl-methacrylate (PMMA) phantom from a single CT scan is measured using a 100mm pencil ionisation chamber ($CTDI_{100}$). Then the dose for the 100mm integrated length is normalised to the nominal beam width. $CTDI_{100}$ is not a point dose measurement but an average dose over a volume of 100mm length. Measurements are performed at the centre and at four peripheral points across the phantom after which a weighted average is calculated ($CTDI_W$) to account for the dose distribution across the central slice of the phantom (x-y plane).

Due to penumbral and scatter effects the radiation profile from a single axial CT scan extends beyond the limits of the collimated scan width. These regions, also known as the scatter tails of the dose distribution, should be included in the $CTDI_{100}$ measurement. That implies that the length of the ionisation chamber should extend beyond these scatter dose tails.

The use of $CTDI_{100}$ has been under investigation lately for both CBCT and mutli-slice CT (MSCT) (Dixon 2003, Mori *et al* 2005, Fearon 2002, Perisinakis *et al* 2007, Jessen *et al* 1999, Brenner 2006, Nakonechny *et al* 2004). Modern MSCT and CBCT scanners offer beam widths that extend far beyond the recommended 100mm integration length of the CTDI definition which makes the use of the CTDI questionable. It has been shown by Dixon (2003), Mori *et al* (2005) and Nakonechny *et al* (2004) that the increasing beam width used by modern MSCT scanners leads to a significant underestimation of the axial (z-axis) dose when measuring the $CTDI_{100}$ because the scatter tails are not fully measured by the 100mm pencil ion chamber.

Different solutions for capturing the entire scatter tail have been proposed, and the current state of the technology leads os to believe that a small-volume ion chamber is the best option currently to measure an appropriate dose index for MSCT in the field (Dixon 2003). However, when considering dentomaxillofacial CBCT, there are a few additional (geometrical, anatomical and practical) issues that need to be taken into account before adapting or defining a suitable dose index:

- Dental CBCT devices exhibit a wide range of field of view (FOV) sizes, ranging from a few cm in diameter to a FOV which can cover the entire diameter of a patients head. In addition, the symmetry of dose distribution throughout the head changes with varying FOV sizes, as smaller FOVs are positioned with a larger distance between the isocentre (*i.e.* the centre of rotation) and the centre of the head for scans focusing on the dental region. The first issue (volume size) has been reported by Boone *et al* (2000) who have simulated the dose distribution of CT scanners in tissues adjacent to an exposed volume. The effect of an asymmetrical rotation centre has been assessed to a limited extent by Lofthag-Hansen *et al* (2008), by performing $CTDI_{100}$ measurements using a small-volume CBCT device.
- Another factor which leads to an asymmetrical dose distribution is the fact that not all CBCT devices expose for a full 360° rotation, as two-dimensional projections acquired from a partial 180°-220° angular range provide sufficient information to reconstruct a three-dimensional volume. This type of exposure can introduce an increased asymmetry to the dose distribution compared to full rotation exposures. Furthermore, a number of devices use the off-axis scanning technique, meaning that the object is scanned using a 'half beam'. This technique results in an overlapping exposed region surrounding the isocenter, leading to further inhomogeneities.
- Additional to the fact that patient dose for dental scans is greatly influenced by the size and position of the FOV, it is also pivotal to acknowledge the influence of the inhomogeneity of the head & neck region, compared to the thoracic and pelvic regions. The complex bony anatomy of the skull may affect the distribution of dose, especially for low-dose scans exposing at a relatively low energy (kVp). Before defining a specific dose index for dental CBCT examinations which is measured in a homogeneous (PMMA or other) phantom, this anatomic influence needs to

be assessed to ensure that measurements performed in this phantom are relevant for patient dose estimation.

- All considerations mentioned above are also relevant for paediatric dose estimations, as all factors affecting the distribution of CBCT dose are particularly relevant for exposures to children. Given the large number of paediatric dental radiographic examinations, it is essential to assess a full and detailed volumetric dose distribution and define a dose index which can be related to both adult patients and children of various ages.
- To continue on the theme of the relevance of a dose index for the estimation of patient dose, the CTDI in general has already been questioned for its relevance for patient risk estimation (Brenner 2006). Again, this critique is especially important for head & neck examinations, as the risk for the patient will be primarily defined by the exposure to a few specific radiosensitive organs at interspersed locations (*i.e.* salivary glands and thyroid gland).
- As a final note, it is practically not feasible to routinely measure the entire z-axis profile for CBCT using a small volume ion chamber. For MSCT scanners, this type of measurement can be performed by one exposure with a sufficiently long scan length. Performing this measurement for dental CBCT requires a large number consecutive scans at changing z-axis positions, with a lag time between scans ranging between less than one minute and several minutes.

All of these pieces of information must be considered when developing a dose index for dental CBCTs. Dose measurements using homogeneous phantoms and anthropomorphic phantoms need to be combined, using different (complementary) dosimetry methods.

In this report, dose measurements in homogeneous water & PMMA phantoms will be presented, involving a number of different CBCT devices and set-ups. Additionally, dose measurements in adult and paediatric anthropomorphic phantoms are presented, and a possible correlation between homogeneous and anatomical phantom measurements is investigated, by comparing dose measurements obtained from water and PMMA phantom to organ and effective doses calculated from anthropomorphic phantoms. These results serve as an evaluation of dose distribution in CBCT, and aid in the definition of an appropriate definition of a CBCT dose index, which can be measured routinely but should be relevant for patient dose estimation as well.

2 The Methodology

2.1 Introduction

In this section, the different methodologies that were used to gather information that is useful for the definition of the CBCT dose index, are presented. Due to the large number of measurements, and the different types of measurement methods and devices used, a general overview of the different measurements will be given.

The first subsection describes the methodology used for measuring a) the scatter tails and b) the dose distributions for different planes. The second section describes the methodology that was used to assess the dose distributions and effective doses in anthropomorphic phantoms.

For the first section, two types of phantoms (test objects) were used for the dose measurements. At the KULeuven, a water phantom was used, comprising a plastic cylinder filled with water, providing a simulation of an average patients head. At UNIMAN, a cylindrical PMMA phantom was developed. Both phantoms allowed different types of dose measurements to be undertaken.

The main portion of the measurements (both in water and PMMA) were performed with thermoluminescent dosimeters (TLDs), which can capture the dose along small areas and can be considered as point measurements. Multiple TLDs (arranged in lines or grids) were used throughout the phantoms to obtain a one-dimensional or two-dimensional view of the dose distribution.

Another tool used is the small volume ion chamber. Because of its accuracy, and the possibility for real-time dose measurement, the ion chamber is a popular tool for medical physicists working in the field. In this study, the chamber was used only with the water phantom, to measure scatter tails (radiation dose outside the primarily exposed area).

Film dosimetry was also performed using the PMMA phantom, which was customized to allow film placement. Film measurements provide high resolution views of the two-dimensional dose distribution, although it has proved difficult to obtain quantitative results from them.

A final dosimetry method involved the use of a dose-area-product (DAP) meter. A DAP-meter is a large area transmission ionisation chamber which is placed perpendicular to the beam central axis and in a location to completely intercept the entire area of the x-ray beam. The reading of the DAP meter is the product of the dose with the beam area and in contrast with absorbed dose, it is independent of the distance from the x-ray source along the central axis. DAP-meters have been extensively used in radiography because they are easy to use and they provide a good estimate of the risk to the patient since they contain information on both the absorbed dose and field size.

Measurements of the first subsection were performed through different planes and lines. For all measurements presented below, the following (conventional) axis system is used: x = front-back, y = left-right, z = down-up. Where necessary, clarification is provided regarding the plane or axis along which the dose was measured. Also, the corresponding anatomical plane is given throughout the descriptions; more information regarding the terminology can be found on section 4.2 of the website below:
http://en.wikipedia.org/wiki/Anatomical_terms_of_location.

The terms 'central positioning' implies that the isocentre (*i.e.* centre of rotation, or centre of reconstructed field of view) is placed at the central axis of the (water or PMMA) phantom. The term 'off-axis positioning' signifies that the isocenter and central axis of the phantom do not coincide.

In the second subsection, three types of phantoms were used, representing an adult, adolescent and child. Because these phantoms are created to resemble the anatomy of a human head, they allow the measurement of dose at different anatomical locations using TLDs, and the subsequent calculation of the effective dose for an average patient. Measurements were performed for different exposure protocols using a wide range of CBCT devices, positioning the phantoms as if they were a patient.

2.2 Measurements using water and PMMA phantoms

In order to assess the scatter tails and the shape of the dose distributions, measurements were performed using a range of dosemeters in water and PMMA phantoms at the two centres (KULeuven and UNIMAN). KULeuven focused on measuring the scatter tails and the dose distributions along the y-z plane, as well as measuring the distribution throughout the x-y plane for a number of exposures. UNIMAN concentrated on measuring the dose distributions along the x-y plane, using a number of CBCT devices, and comparing protocols for central and off–axis positioning, and full and partial rotations.

2.2.1 Measurements in water phantom (KULeuven)

To evaluate the distribution of radiation dose in a homogeneous phantom, a plastic cylinder of 15cm diameter and 25.5cm height was selected. It was filled with water, enabling measurements of primary and scattered radiation at various positions using thermoluminescent dosimeters (TLDs) and an ionisation chamber. The type of TLDs used in this study was TLD-100 (LiF:Mg,Ti). The ionization chamber (Farmer type) used in this study has a volume of 0.6cm^3 and consists of a graphite wall with a thickness of 0.4mm. The TLDs are very small (9mm²) in size and are used to make point measurements but they are not as accurate as the ionization chamber.

TLD measurement of y-z (coronal) plane, central positioning

For this measurement, 154 TLDs were placed in the water phantom in a vertical grid pattern at 1 cm intervals (Figure 1). The grid contained 11 rows

and 14 columns, spanning an area of 130 cm². It was placed perpendicular to the X-ray beam on the y-z plane (midcoronal plane). The grid was exposed with the SCANORA 3D CBCT unit, using the standard protocol for adult patients (Appendix 1). The isocentre of the x-ray beam was positioned at the midpoint of the grid (both horizontally and vertically), which coincided with the midpoint of the cylinder. After read-out of the TLDs, the distribution of radiation dose throughout the grid was evaluated.

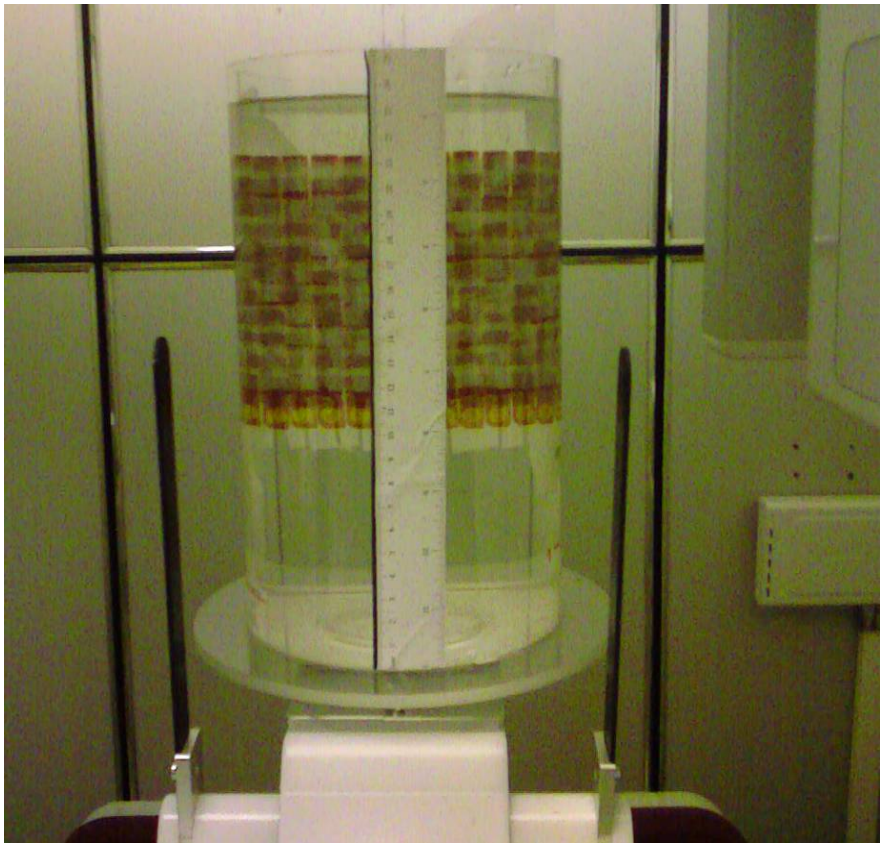

Figure 1. TLD measurement in water phantom with central FOV positioning, showing 14x11cm TLD grid positioned along the y-z plane.

TLD measurements of y-z (coronal) plane, off-axis positioning

In a first evaluation of off-axis positioning, the SCANORA 3D's small field was used, using standard exposure settings (Appendix 1). The field was positioned non-centrally, with the isocentre placed at 5 cm from the central point of the cylinder, mimicking a dental examination (incisor/canine region). For this measurement, a grid of 76 TLDs was used. This grid contained 4 columns of 19 TLDs each, interspaced at 1 cm. Due to z-axis symmetry, the columns could be positioned on one side of the central x-y plane, covering coordinates from z=0cm up to z=18cm. This way, as in the first measurement, the shape and extent of the axial scatter tail could be determined (which was also facilitated by selecting a FOV with a smaller height). The 4 columns were positioned with variable intervals along the y-axis: centrally in the FOV, 1.5 cm from the isocentre (on the midpoint between the isocentre and border of the FOV), and at 4.5cm and 6cm from the isocentre (both outside the FOV).

For a second evaluation, the 3D Accuitomo XYZ was used. This device uses a small-sized FOV of 4x3cm, which further enables the determination of the dose distribution along the z-axis and at positions that are outside the FOV but inside the primary beam for part of the exposure. For this measurement, a TLD distribution was used similar to the previous with a grid of 76 TLDs divided into 4 columns with a 1cm interspace along the z-axis. The isocentre was placed at 5.5cm from the centre of the cylinder. The placement of the columns was adapted to obtain the same relative positions compared to the previous measurement (*i.e.* at 0cm, 1cm, 3cm and 4cm from the isocentre). Default patient exposure settings were used (Appendix 1).

Ion chamber measurements of y-z (coronal) plane, central positioning

In addition to the TLD measurements, ion chamber measurements were performed on the SCANORA 3D (Appendix 1) at 1cm intervals along the z-axis, combining central, midperipheral and peripheral measurements with measurements outside the FOV, all in the y-z plane. Measurements were repeated for each position to check for consistency, and corrected for temperature and pressure.

TLD measurements of x-y (axial) plane

As a final evaluation of dose distribution within the water phantom, 69 TLDs were positioned in a grid pattern in the XY-plane. This type of measurements closely resembles those performed in the PMMA phantom, described below. The distance between adjacent TLDs in any row was 2cm, and adjacent rows were shifted 1 cm. Measured values were inserted into a 13x13cm matrix, and empty cells were interpolated (Figure 2).

Measurements were performed on three CBCTs. For the Scanora 3D off-axis positioning was used. For the GALILEOS, a partial rotation in combination with an off-axis exposure was measured. For the Illuma, a high and low dose protocol was measured using central and off-axis positioning, respectively. Exposure factors can be found in Appendix 1.

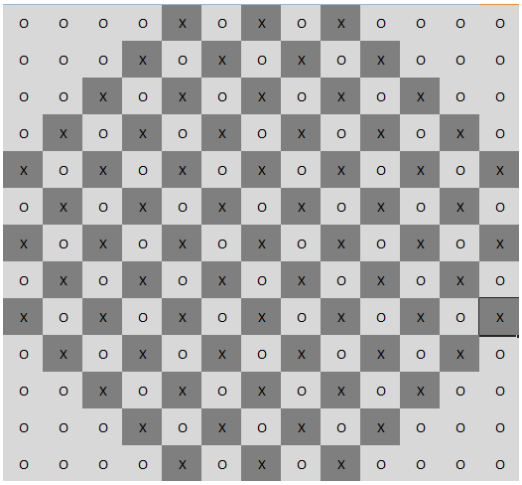

Figure 2. Positioning of TLDs in XY (axial) plane for water measurements. The distance between adjacent TLDs is 3cm. Dark grey (X): TLD position, light grey (O): interpolated value. Values in the four corners are interpolated for graphing purposes and have no significance, as they fall outside the phantom.

2.2.2 Measurements in PMMA phantom (UNIMAN)

This section describes the methodology that was used to measure and visualize dose distributions along the x-y plane for a range of dental CBCT systems. Although these measurements are comparable to some degree to the x-y measurements in the water phantom described above, the PMMA measurements provide a direct comparison of a wide range of CBCT devices and protocols.

The PMMA phantom was designed by the Manchester team and was manufactured by Leeds Test Objects (Figure 3). It consists of 7 interchangeable slices of 16cm diameter and 2.8cm thickness (Figure 4). The slices are designed to fit into each other. Two additional slices were manufactured for TLD and film dosimetry (Figure 5). An extra disc positioned at the top of the phantom was designed to allow alignment of the phantom with the laser beams of the dental CBCT units (Figure 6). Final designs were submitted on 11th March and the phantom was delivered on 21st May. The TLDs are positioned 3 cm apart (Figure 5 and Figure 7). For each exposure setting 37 TLDs were used as shown in Figure 5.

Dose distribution measurements were performed on an 3D Accuitomo 170, NewTom VG, i-CAT Next Generation and ProMax 3D using TLD-100H (LiF: Mg, Cu, P). The TLDs were individually calibrated against an ionization chamber. Their energy response was evaluated and it was found to be flat. A large number of exposure geometries (axis and off-axis, FOV diameter & height) were used. Where possible, TLD measurements were accompanied by dose-area-product (DAP) measurements and radiochromic film measurements. Radiochromic films were used because they are light insensitive and do not have to be inserted in a film cassette or black envelope. The films were used to visualize the two dimensional image of the dose distribution.

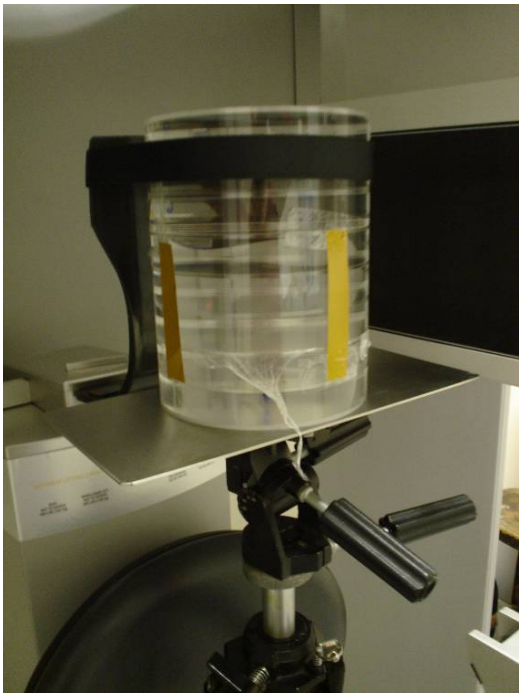

Figure 3. PMMA phantom in position for measurement

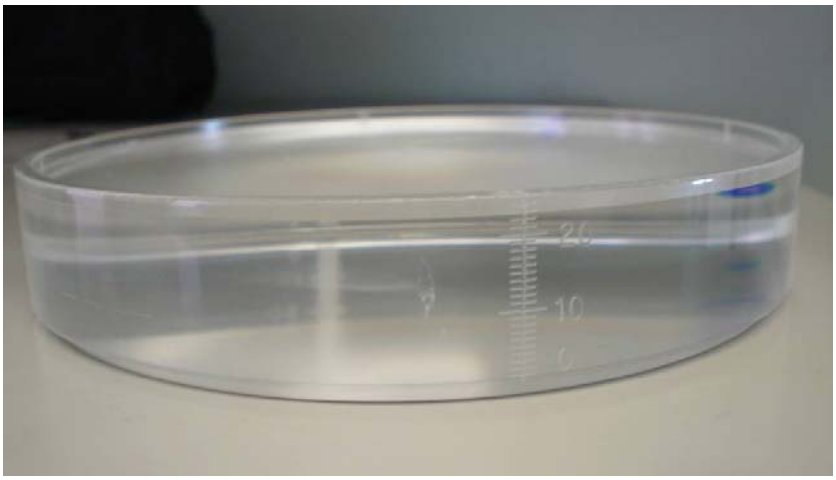

Figure 4. PMMA slice

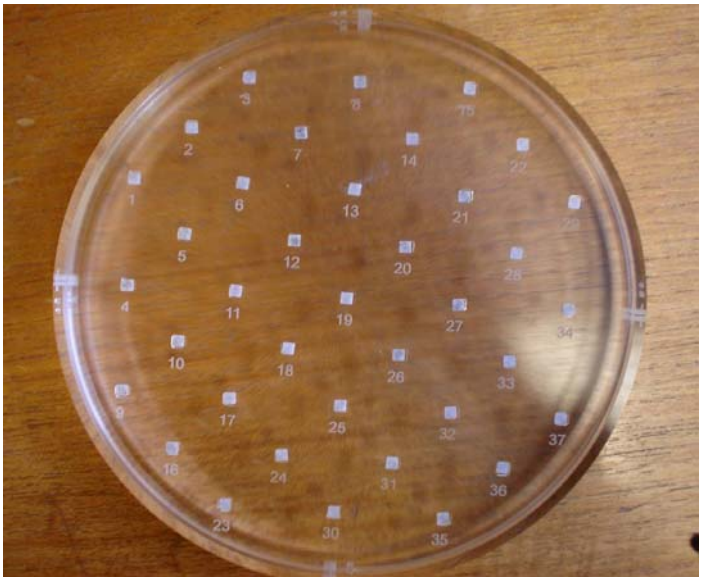

Figure 5. PMMA slice loaded with TLDs

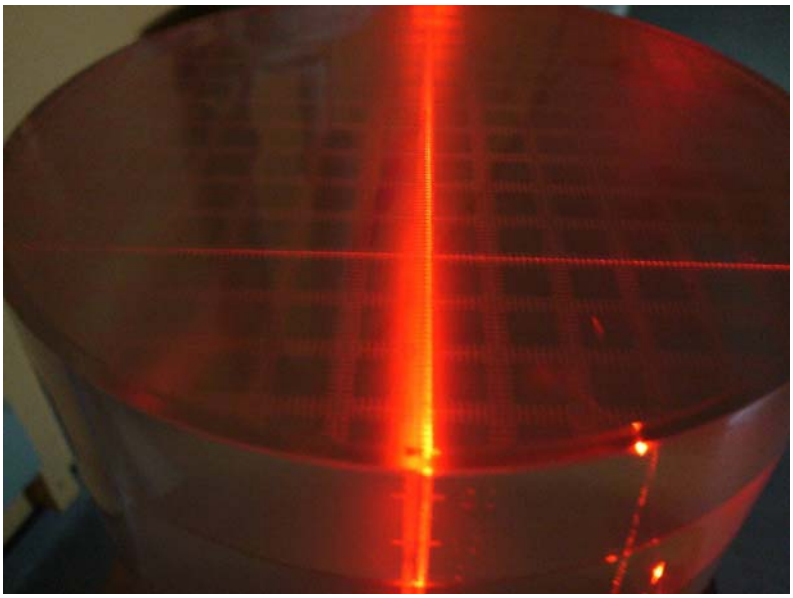

Figure 6. PMMA top disc on top of the phantom to allow accurate positioning

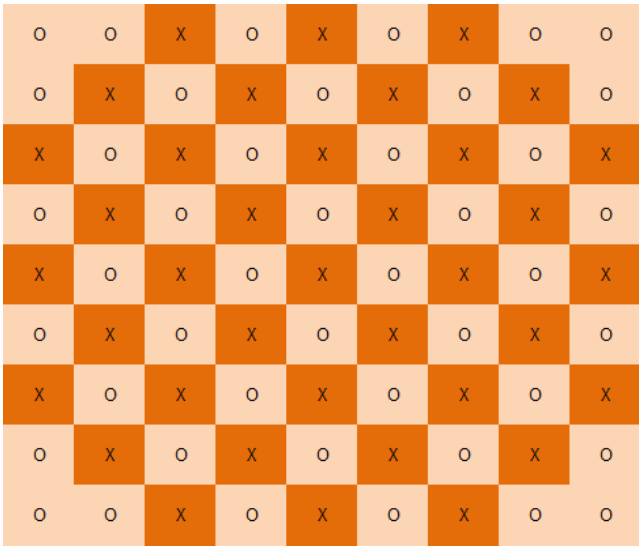

Figure 7. Positioning of TLDs in x-y plane for PMMA measurements. The distance between adjacent TLDs is 3cm. Dark orange (X): TLD position, light orange (O): interpolated value. Values in the four corners are interpolated for graphing purposes and have no significance, as they fall outside the phantom.

2.3 Measurements in anthropomorphic phantom (KULeuven & UNIMAN)

To estimate the effective dose for an average adult male, two similar types of anthropomorphic male Alderson Radiation Therapy (ART) phantoms (Radiology Support Devices Inc., CA, USA) were used (Figure 8). It represents an average man (175 cm tall, 73.5 kg) and consists of a polymer mold simulating the bone, embedded in soft tissue equivalent material. It is transsected into 2.5 cm thick slices, each containing a grid for TLD placement. As the dose in the lower part of the phantom has been reported as negligible compared to the dose in the upper part for dental low-dose CT examinations (Loubele *et al* 2006), dose level assessment was only performed on the upper 11 slices corresponding to the head and neck region.

Figure 8 ART adult male phantom

For the estimation of paediatric dose, two tissue-equivalent anthropomorphic phantoms (ATOM Model 702-C and ATOM Model 706-C, Computerized Imaging Systems, Inc, USA) were used. Models 702-C and 706-C simulate an adult female and a 10 year old child respectively. An adult female phantom was used to simulate a teenager as there are no commercially available teenager tissue equivalent anthropomorphic phantoms. The ATOM phantoms are based on ICRP 23 and ICRU 48 and available anatomical data. The tissues simulated in the ATOM phantoms are average bone and soft tissue, cartilage, spinal cord, spinal disks, lung, brain, sinus, trachea and bronchial cavities. The paediatric simulated bone tissues match age related density. The bone tissue is an average of known cortical to trabecular ratios and age based mineral densities. The ATOM phantoms are available in 25 mm slices and for the purposes of this study the head, neck and shoulders of both phantoms were used as shown in Figure 9.

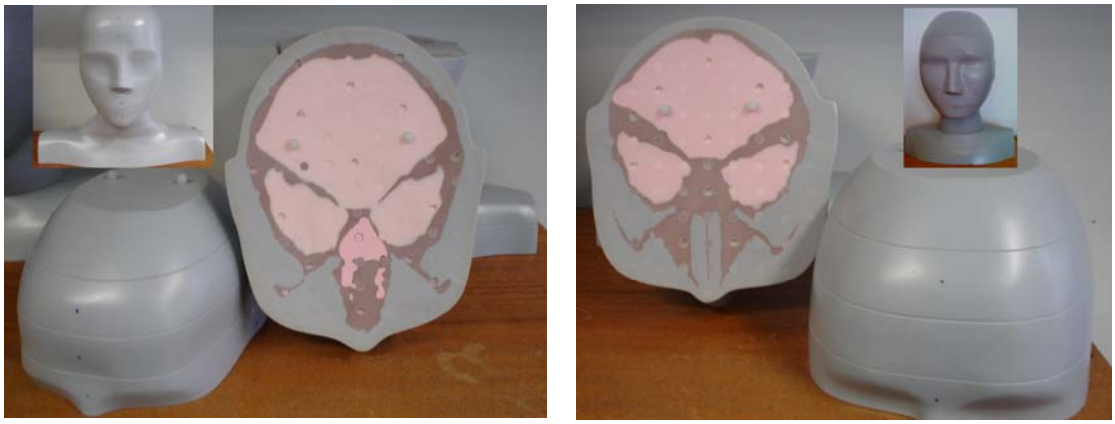

Figure 9. ATOM Models 702-C and 706-C

Measurements were performed on all phantoms by inserting TLDs at different positions within different slices of the organs or tissues of interest. For each slice, placement of the TLDs was carefully considered to ensure that there was an even spread over the different radiosensitive organs for each slice.

The phantoms were scanned on a variety of available CBCT devices, combining different exposure protocols when possible. The phantoms were irradiated a number of times to enlarge the dose substantially above the background dose, which was measured using non-irradiated TLDs and subtracted from all field TLD values. In order to calculate the equivalent dose HT for all organs or tissues T, the following formula was used:

$$H_T = w_R \Sigma f_i D_{Ti}$$

with w_R the radiation weighting factor, being 1 for x-rays, D_{Ti} the average absorbed dose of organ T in slice i, and f_i the fraction of organ T in slice i. For all organs except the skin, red bone marrow and bone surface, calculation of H_T was straightforward since the organs are found either completely within the head and neck or completely outside, as opposed to bone and skin which are present throughout the whole body. For the latter, the organ fractions reported by Huda *et al* (1984) were used. The equivalent organ dose has to be multiplied by the tissue weighting factor w_T to obtain the contribution E_T of the organ to the effective dose.

$$E_T = w_T \cdot H_T$$

Summing all contributions E_T thus provides the effective dose E.

3. Results

3.1 Introduction

The results will be presented in three subsections, similar to those of the methodology section. First, the water phantom measurements will be shown, containing TLD and ion chamber measurements of the water phantom along different planes. Next, PMMA phantom measurements of the x-y plane are presented. Also, in this subsection, corresponding film dose distributions and dose-area-product (DAP) measurements are given. In the final part of the results section, anthropomorphic phantom measurements are shown.

3.2 Measurements using water and PMMA phantoms

3.2.1 Measurements in water phantom (KULeuven)

Measurements in water phantom along z-axis and x-z plane

Figure 10 shows ion chamber dose values at different coordinates, using a central position of the SCANORA 3D device. The absorbed dose within the FOV was within a range of 2.0-2.5 mGy. A drop in dose values can be perceived when measuring at coordinates which are outside the primary beam area at all times. This drop is gradual because the ion chamber, which measures the dose of a certain volume, gradually moves out of the primary beam.

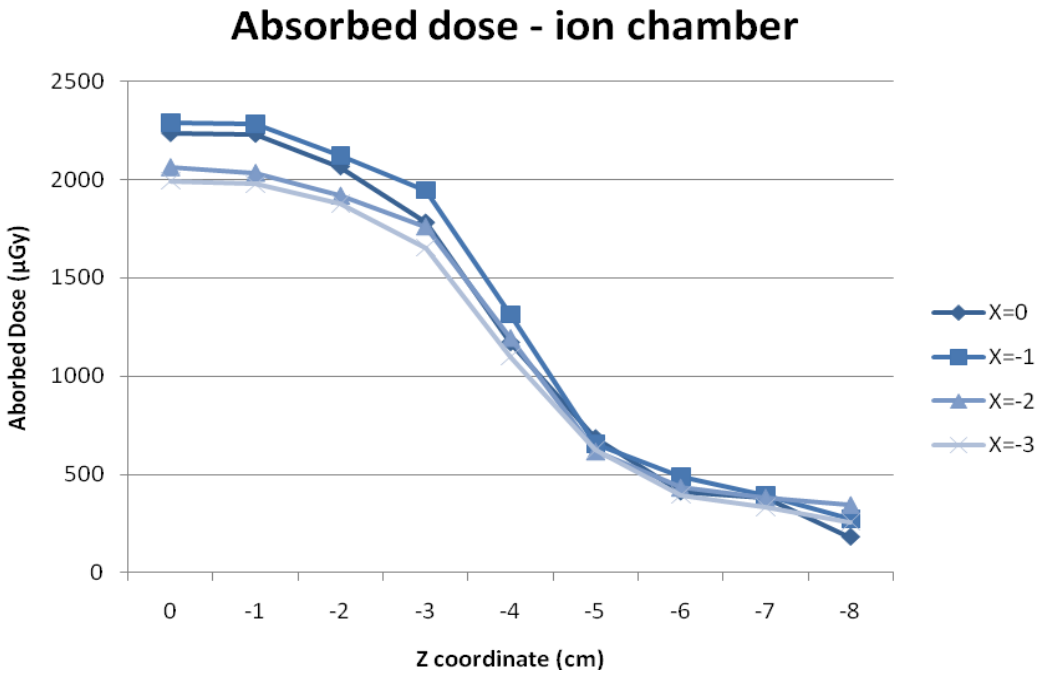

Figure 10. Absorbed dose measurements from ion chamber in water phantom, using an FOV of 100x75cm (z coordinates higher than 3.75 are outside the FOV). Four different data series are shown, depicting measurements along the z-axis for different x-coordinates.

Figure 11 shows a surface plot of the dose distribution in water measured by TLDs using a 14x11 grid and positioning the phantom centrally in the SCANORA 3D's FOV. The plot is also shown from the frontal perspective (showing the distribution along the x-axis) and the lateral perspective (showing the distribution along the z-axis). Generally, absorbed doses within the field of view are between 2.0 and 2.8 mGy. Doses are highest in the isocentre, and remain high along the x-axis, even when measuring outside the reconstructed volume. Along the z-axis, a clear drop in dose values is shown outside the primary beam area, although the evaluated area is not wide enough to get a clear view on the amount of scattered radiation along this axis.

The absorbed dose for asymmetrical positioning of the water phantom in the SCANORA 3D and 3D Acccuitomo is depicted in Figure 12 and Figure 13, respectively. Similar results can be observed for both CBCTs, even though there is a large difference found for the absorbed dose within the FOV (SCANORA 3D 1.5-3.0 mGy, 3D Accuitomo 4.0-7.5 mGy). Compared to the previous TLD measurement and the ion chamber measurements, additional information is obtained. The scatter tail is shown more extensively, demonstrating a clear, but smooth drop in dose when measuring outside the primary beam. It is seen that there can be a noticable dose deposition just above or below the FOV. However, there is no exact information regarding the extent of overscanning, although the exact exposed area can be measured or verified straightforwardly using radiochromic film. The scatter tails are shown to extend to a distance of twice or more the height of the FOV, confirming the previously mentioned consideration that the 100mm pencil ion chamber would be inadequate to capture the entire scatter tail.

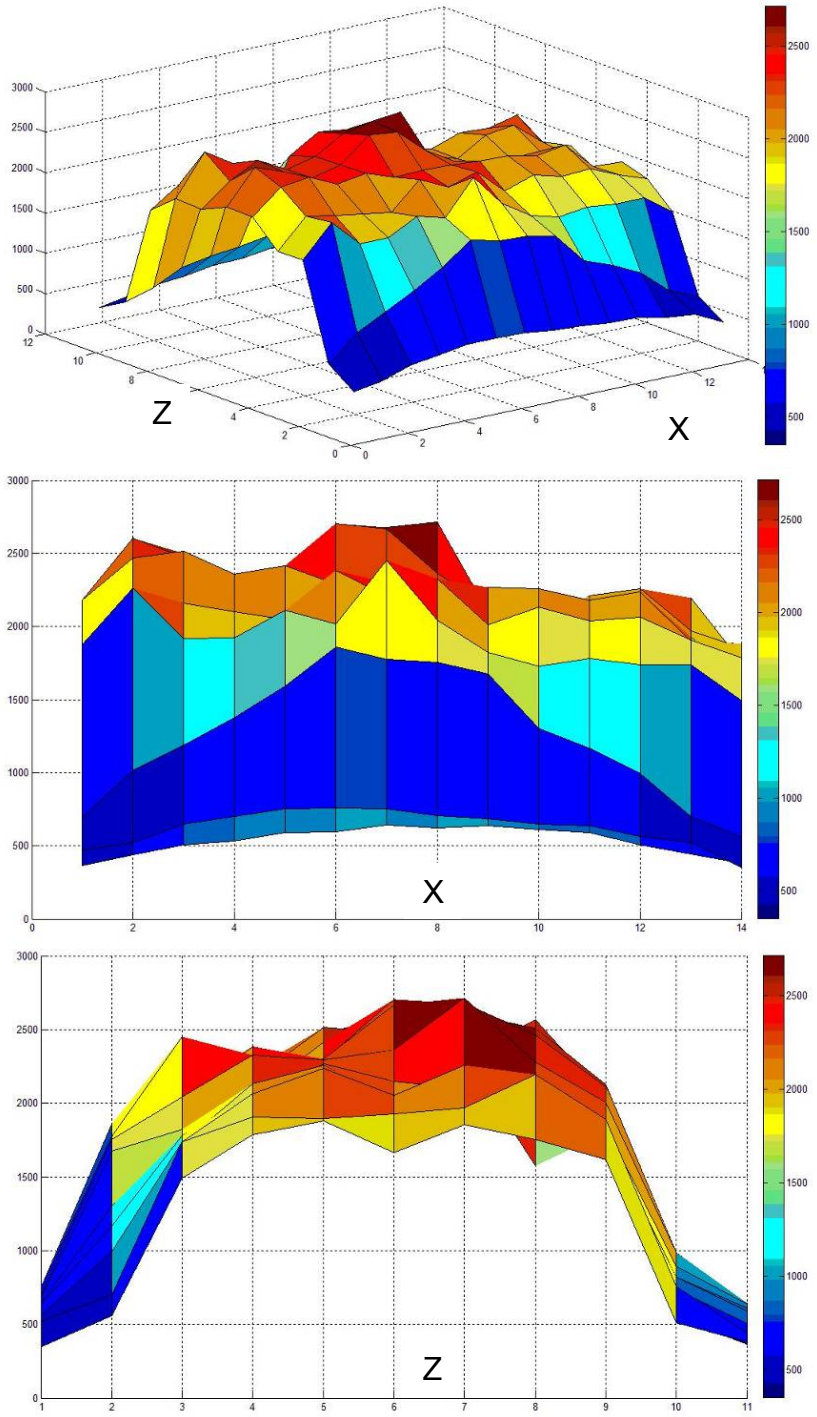

Figure 11. Surface plot of TLD measurements in water. Dose values are in µGy. The FOV was positioned centrally in the water phantom, and TLD measurements were performed symmetrically around the isocentre. Top: overview showing 2D distribution of dose in the x-z plane, y=0. Middle: dose distribution along the x-axis. Bottom: dose distribution along the z- axis.

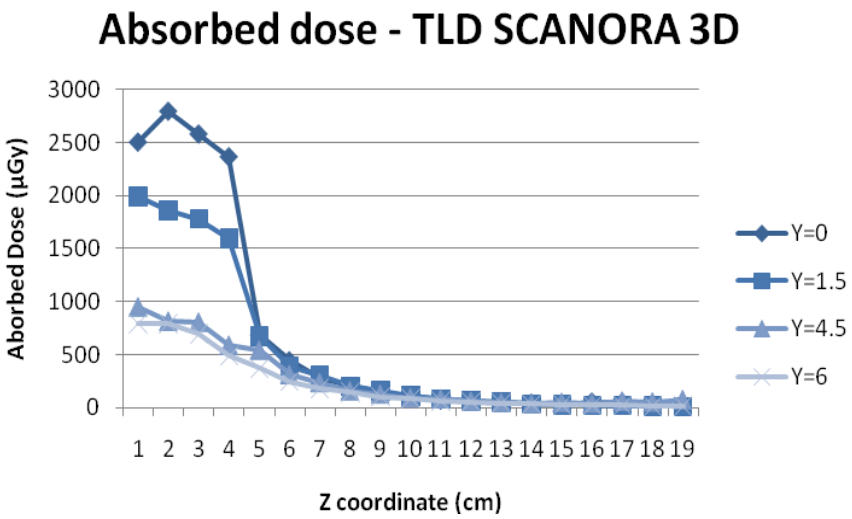

Figure 12. Absorbed dose measurements from TLDs, using asymmetrical isocentre positioning on the SCANORA 3D CBCT (isocentre at z=0, field border at z=3.75cm)

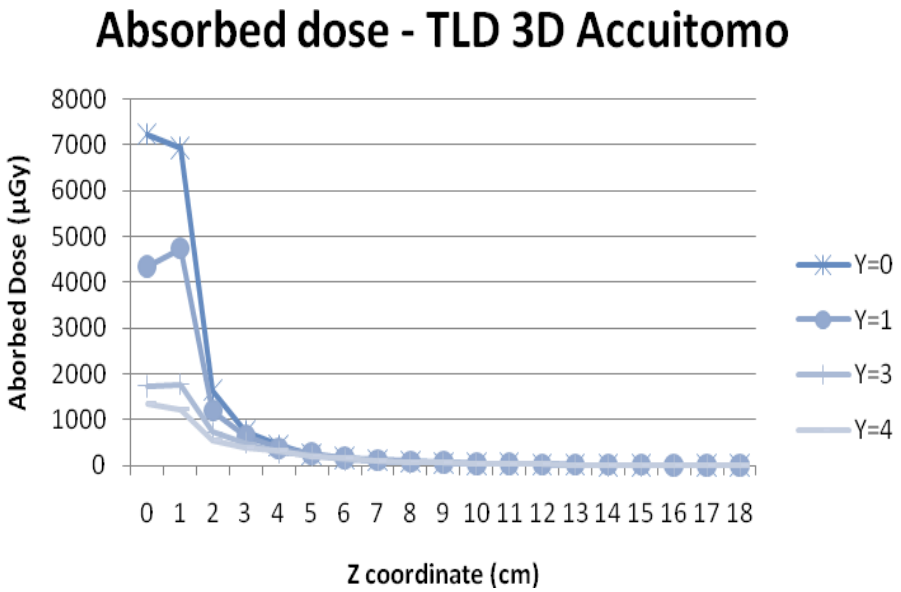

Figure 13. Absorbed dose measurements from TLDs, using asymmetrical isocentre positioning on the 3D Accuitomo CBCT (isocentre at z=0, field border at z=1.5cm)

Measurements in water phantom of XY-plane

Four different measurements, using three CBCT devices are shown in All graphs are shown as the percentage of the maximum dose and they are colour-coded surface plots. As shown on the graph, the bottom of each 2D distribution represents the front (anterior) side of the phantom, whereas the left side of the graph corresponds to the left side of the phantom. As seen on the figure, only one scan shows a more or less homogeneous distribution, as it is a 360° scan with central positioning and a large FOV. All others exhibit a

gradient of dose (which can be higher in the anterior region or vice versa), due to either a partial rotation or off-axis positioning. Also, a peculiar left-right asymmetry can be seen for the SCANORA 3D, which cannot be directly explained. It can partly be due to a small positional error (rotation of the phantom towards the right side). Another factor could be that the SCANORA 3D uses half beam scanning, although this should lead to a dose peak in the overlapping region, rather than a left-right asymmetry.

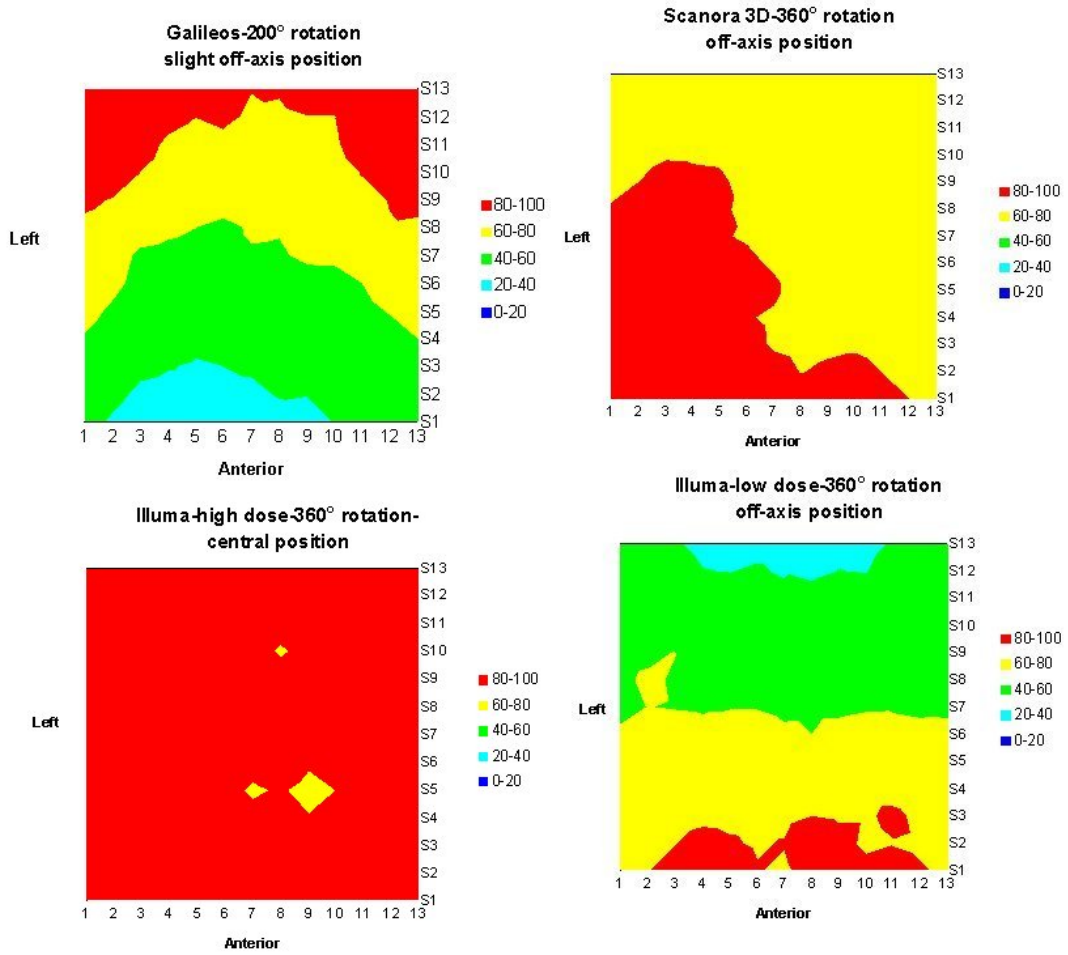

Figure 14. Relative dose distributions (%) at the x-y plane for different CBCT units and exposure settings

3.2.2 Measurements in PMMA phantom (UNIMAN)

Figure 15 shows the dose distribution for three protocols of the ProMax 3D. The dose distributions were not uniform for all three measurements because the device does a 220° rotation instead of a full rotation around the patient's head. The dose distributions for the small and large FOVs are similar. The highest dose area is shifted to the back at the back and right of the phantom with two hot spots at similar positions in the two set-ups. For the off-axis positioning, the dose distributions was more uniform in the central region of the phantom than for the other two measurements but at the front and back of the phantom there were two hot spots.

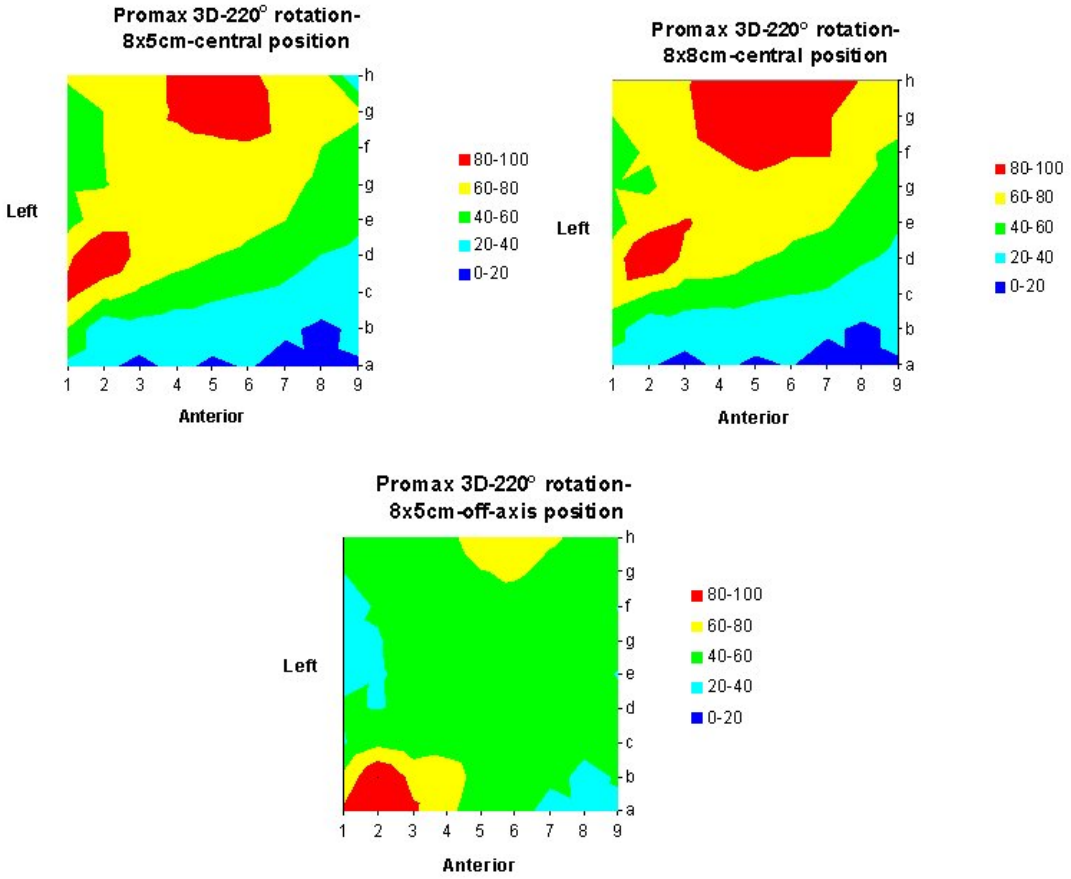

Figure 15. Relative dose distributions (%) at the x-y plane for the Promax 3D

The dose distributions for the NewTom VG, along with the film dose distribution, are shown in Figure 16.

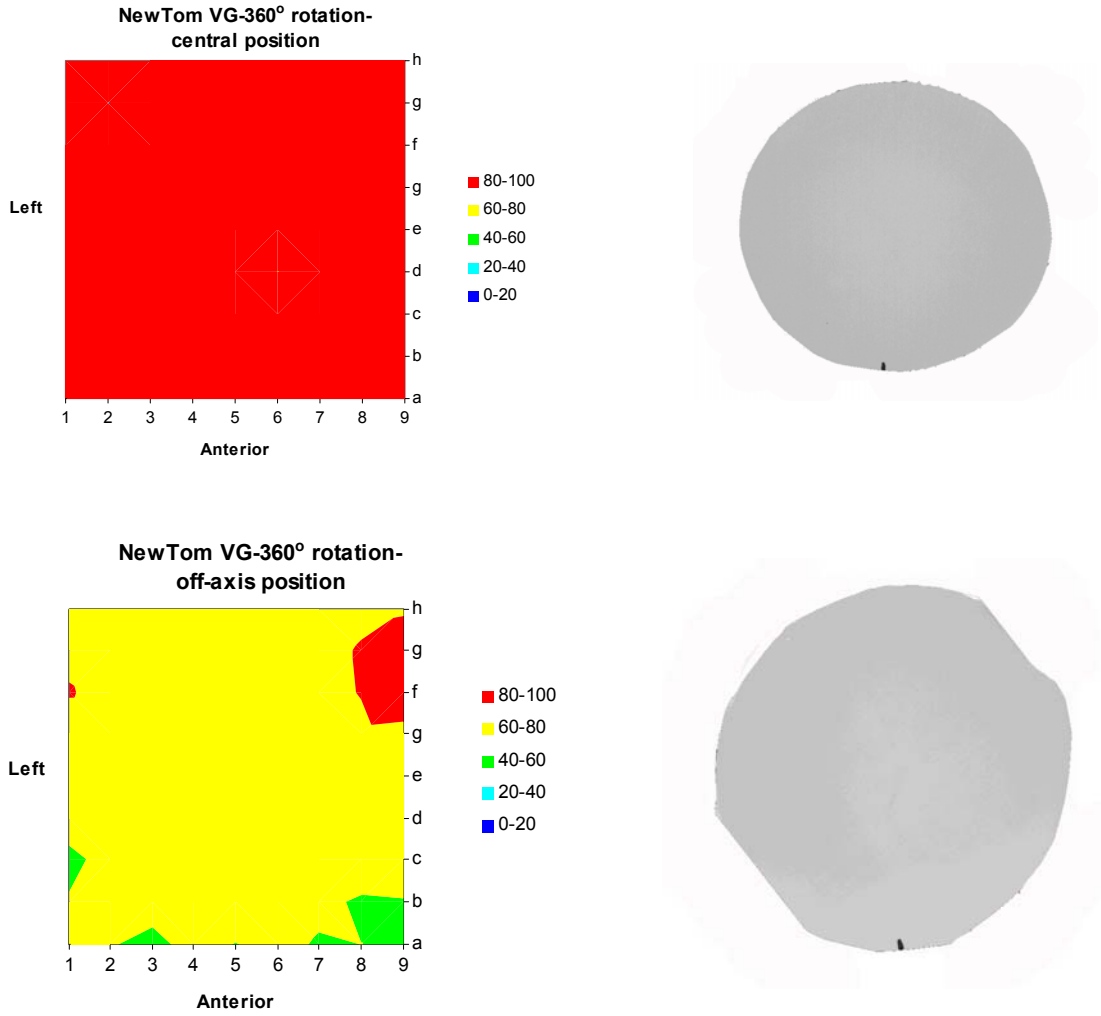

Figure 16. Relative dose (%) and film distributions at the x-y plane for the NewTom VG

These distributions show a homogeneous dose distribution for central positioning, and a front-back dose gradient for off-axis positioning.

Figure 17 and Figure 18 show the dose distributions for all Accuitomo protocols. Large differences can be seen between the different protocols, due to variations in field size, rotation, and positioning.

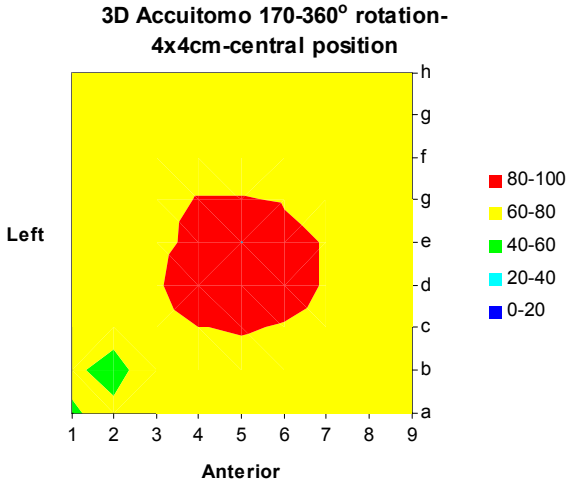

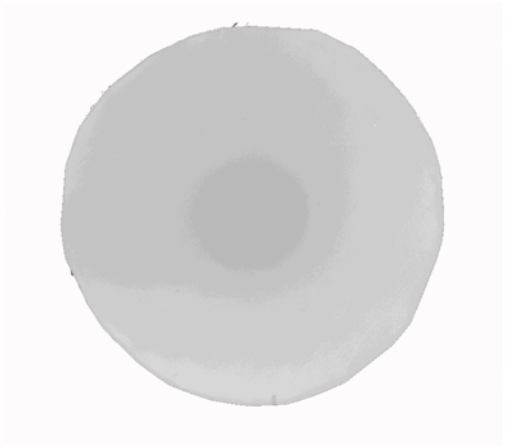

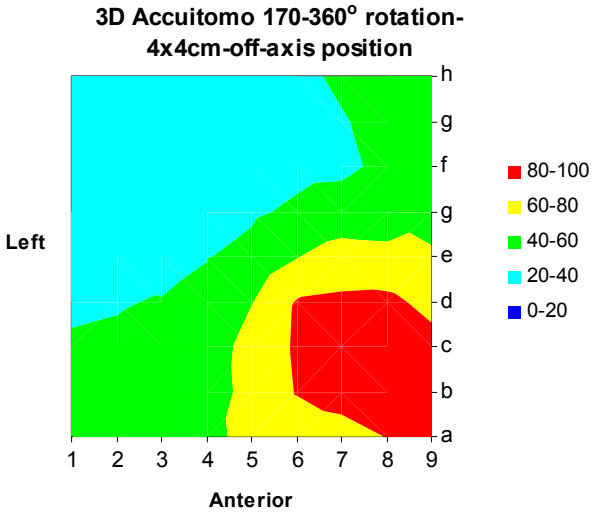

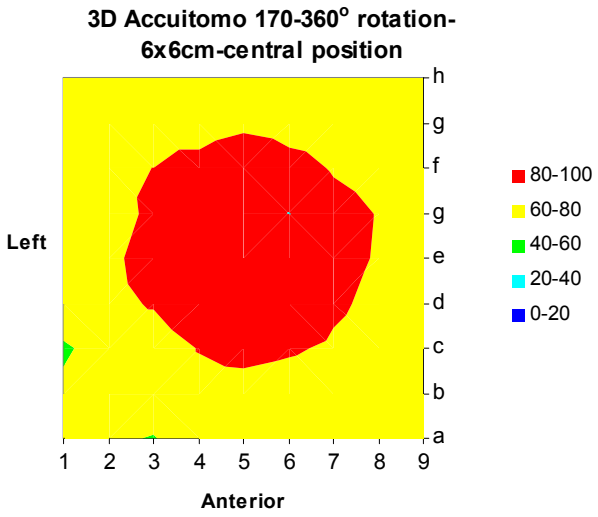

Figure 17. Relative dose (%) and film distributions at the x-y plane for the 3D Accuitomo 170 and for small field of views

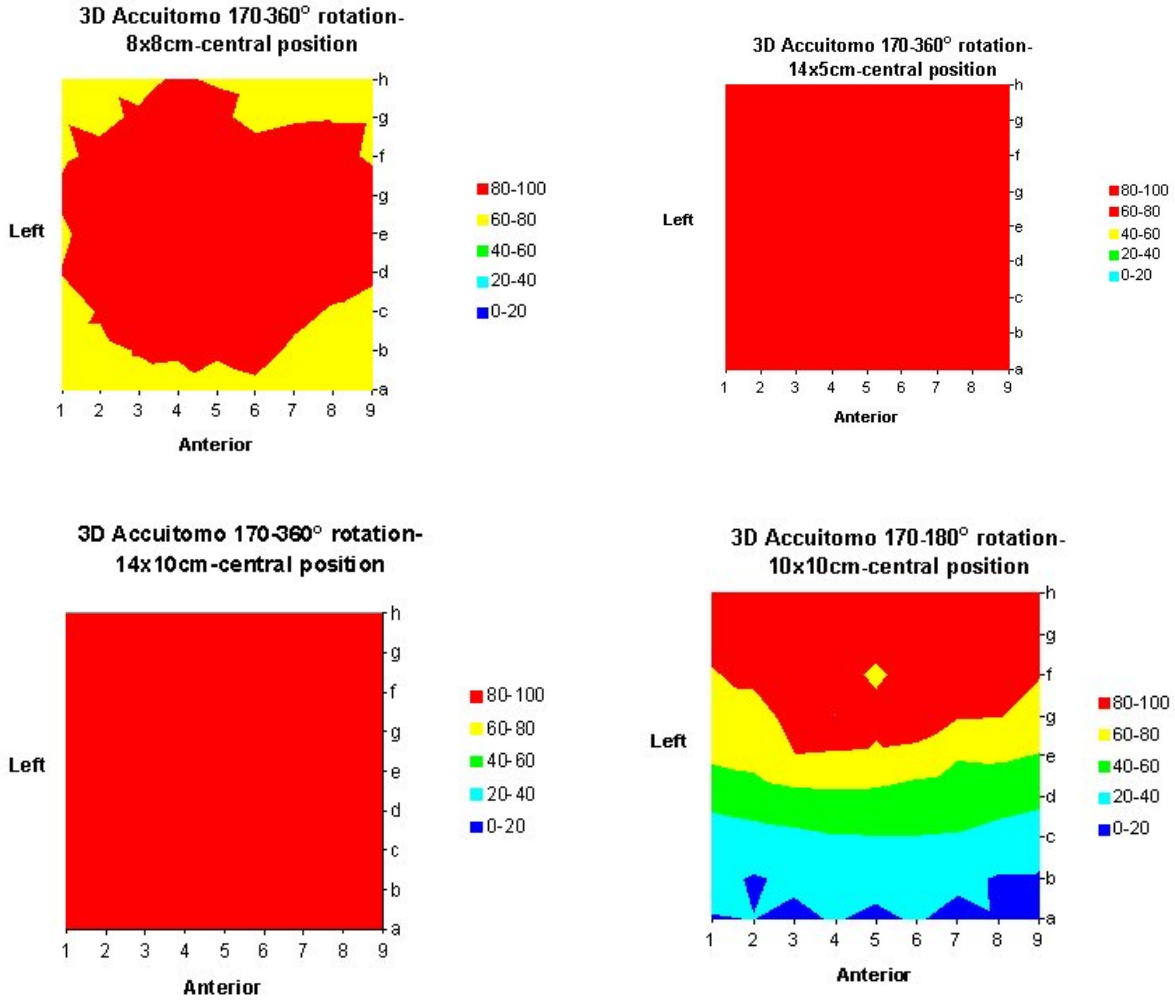

Figure 18. Relative dose (%) and film distributions at the x-y plane for the 3D Accuitomo 170 and for large field of views

Dose distributions for all i-CAT protocols are shown in Figure 19 and Figure 20. Again, there is a clear change in dose distributions when scanning using half a rotation, or by scanning the phantom off-axis.

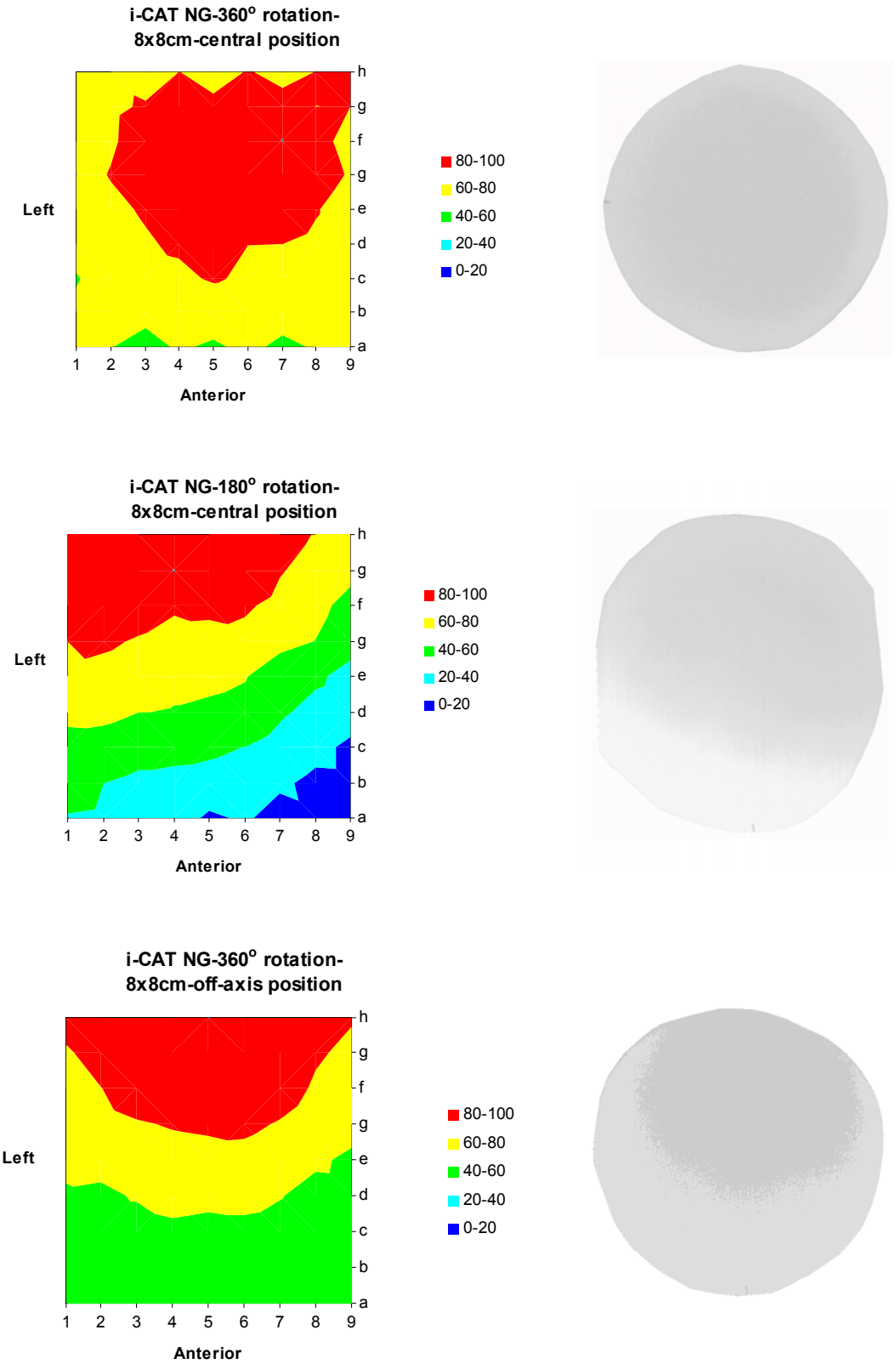

Figure 19. Relative dose (%) and film distributions at the x-y plane for the i-CAT NG and for small field of views

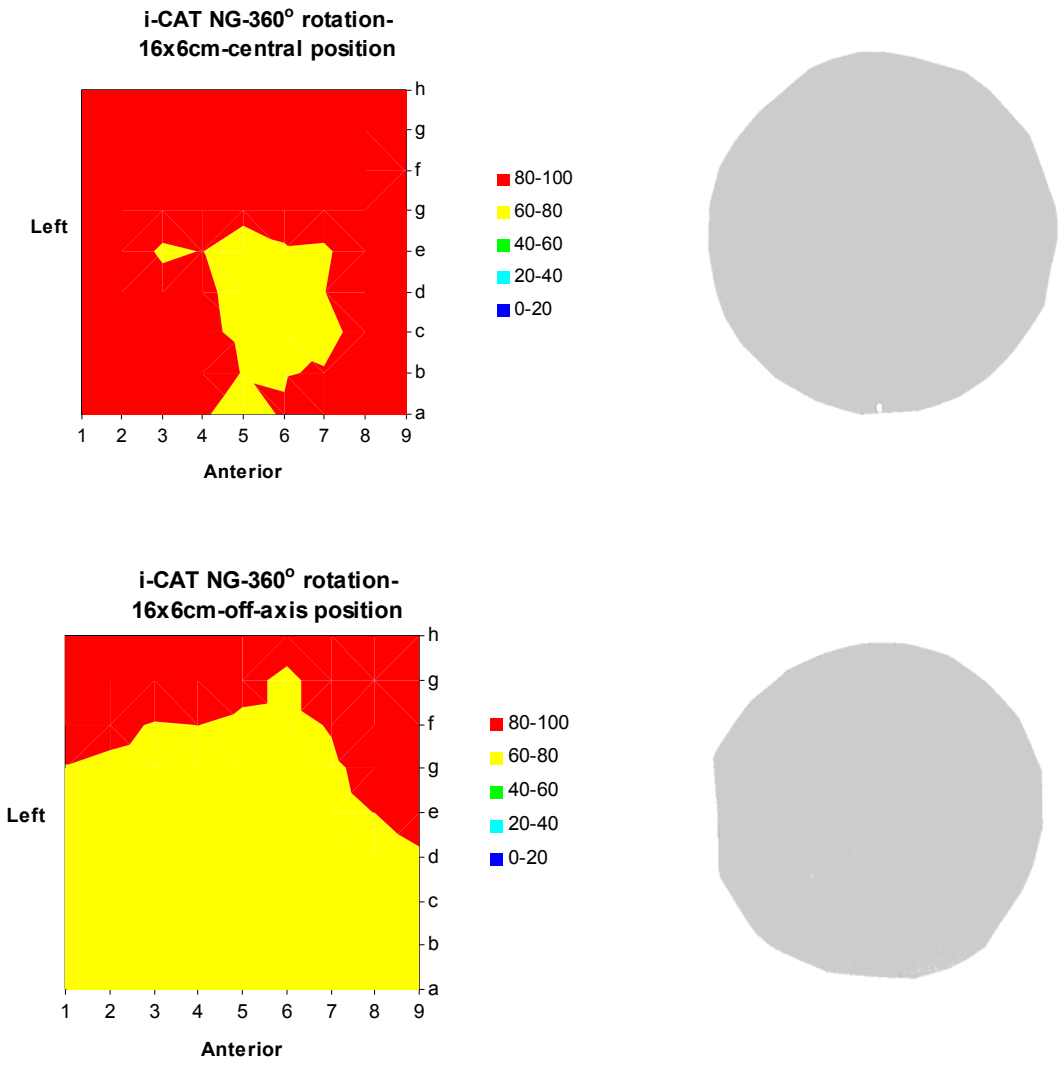

Figure 20. Relative dose (%) and film distributions at the x-y plane for the i-CAT NG and for large field of views

Dose area product measurements (UNIMAN)

Table 1 shows the DAP and average TLD values obtained from the x-y plane dose distributions for all measured protocols for the 3D Accuitomo 170 and for the i-CAT Next Generation. There is a range of DAP values covered by the two systems. Figure 21 and Figure 22 show that there is a non-linear relationship between the DAP values and TLD average dose. The latter will obviously show a positive relation with the FOV diameter when keeping other exposure parameters constant. The non-linear relationship between the DAP values and the average dose in the mid axial slice should be further investigated by expanding the measurements to more systems and exposure settings. Establishing a relationship between the DAP and dose for each system could aid in the determination of a relation between DAP and effective dose.

Table 1. DAP values for different CBCT devices and protocols

	DAP (µGym^2)	Average dose TLD (mGy)
3D Accuitomo 170		
4Øcm x 4 cm height	29,59	2,3
6Øcm x 6 cm height	62,73	3,89
8Øcm x 8 cm height	98,6575	4,81
10Øcm x10 cm height	135,67	6,34
10Øcm x 5 cm height	74,44	5,25
i-CAT NG		
16Øcm x 6cm height	20,73	1,44
16Øcm x 8cm height	39,9	1,89
8Øcm x 8cm height	27,74	1,6
16Øcm x 10cm height	31,52	1,87
16Øcm x 16cm height	44,42	1,98

The following figures show the relationship between the DAP and the average dose obtained from the TLDs for the CBCT scanners.

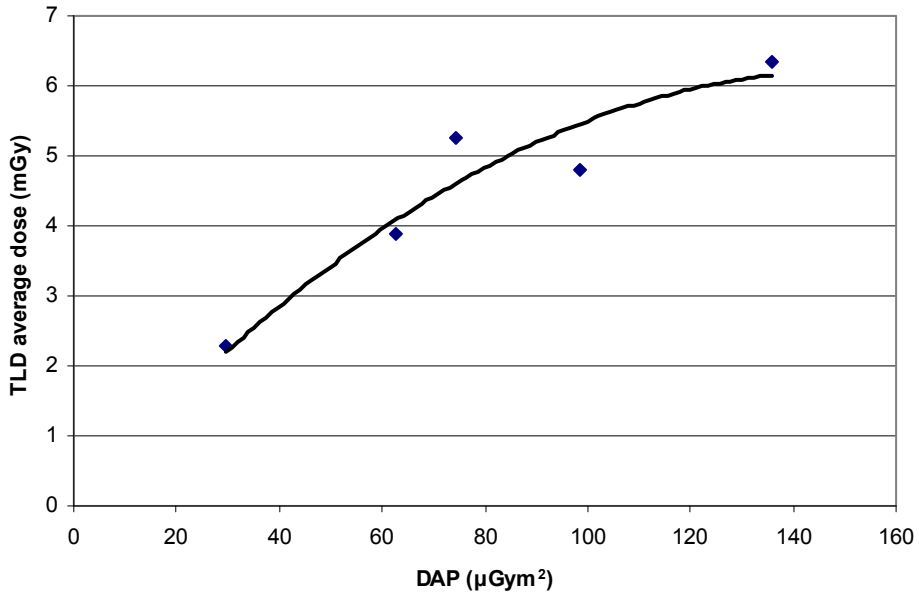

Figure 21. Relationship between the DAP and average dose for the 3D Accuitomo

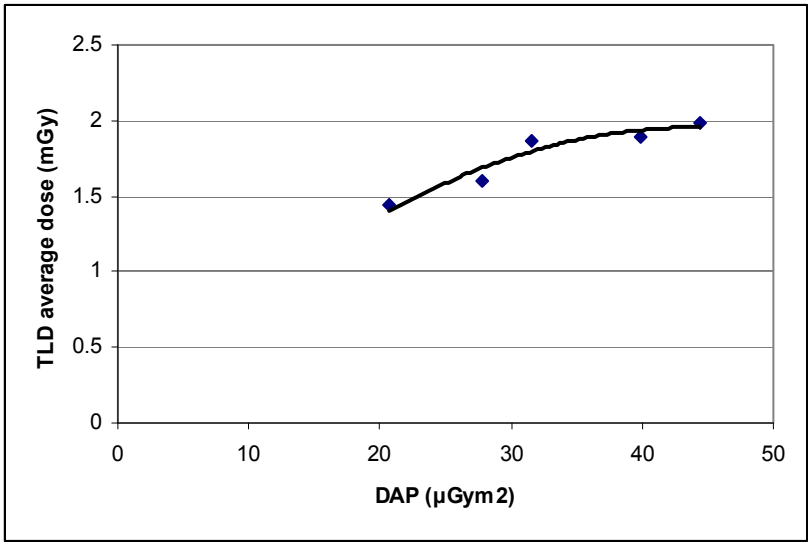

Figure 22. Relationship between the DAP and average dose for the i-CAT NG

3.3 Measurements in anthropomorphic phantom (KULeuven & UNIMAN)

Figure 23 shows the organ absorbed doses to different organs for the ART adult phantom. The effective doses are illustrated in Figure 24. The salivary and thyroid glands receive the highest organ doses. They are positioned between slices 5 and 8 and between slices 9 and 10 respectively. The salivary glands are either partially or fully irradiated by the primary beam depending on the clinical examination. The thyroid gland is either exposed to scattered radiation and/or is partially irradiated by the primary beam. The absorbed doses to skin, red bone marrow and bone surface were rather small due to the fact that only a fraction of the total mass of these organs is located in the head and neck region of the phantom. Figure 23 shows that there is a wide variation in the absorbed doses for all the organs. This is due to a) the clinical area being imaged and b) the wide range of exposure factors set by the manufacturers and clinical staff (Appendix 1).

The salivary glands, thyroid gland and the red bone marrow are the three organs that contribute the most to the effective doses for all the CBCT units and clinical examinations. Although the dose to the red bone marrow is much smaller than the salivary and thyroid glands doses, its contribution to the effective dose is significant due to its high radiosensitivity.

Figure 24 shows that there is a wide range of effective doses even for the same clinical indication, with an average value of 43 µSv. This is mainly due to the exposure factors set by the manufacturers and clinical staff. The highest and lowest effective doses correspond to the ProMax 3D and i-CAT Next Generation units. Galileos, Picasso Trio and NewTom VG use relatively large FOVs resulting in effective doses greater than 50 µSv. It should be noted that the exposure factors used for this study were those selected by the users to give acceptable image quality for a standard patient.

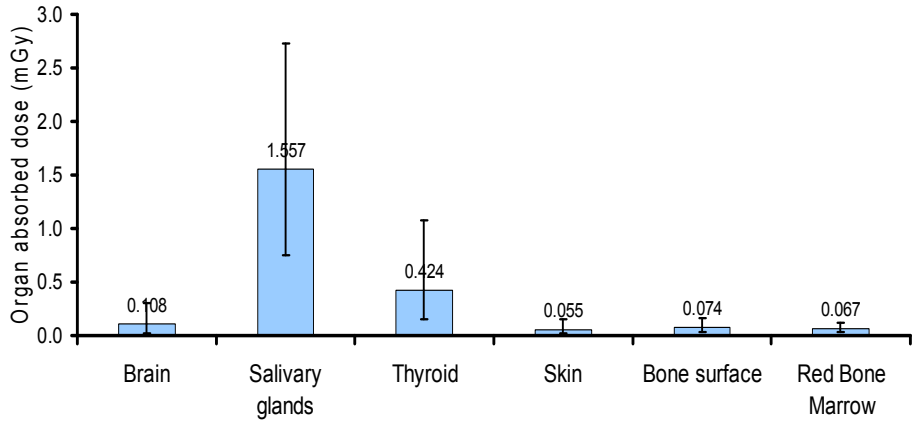

Figure 23. Average, minimum and maximum absorbed organ doses

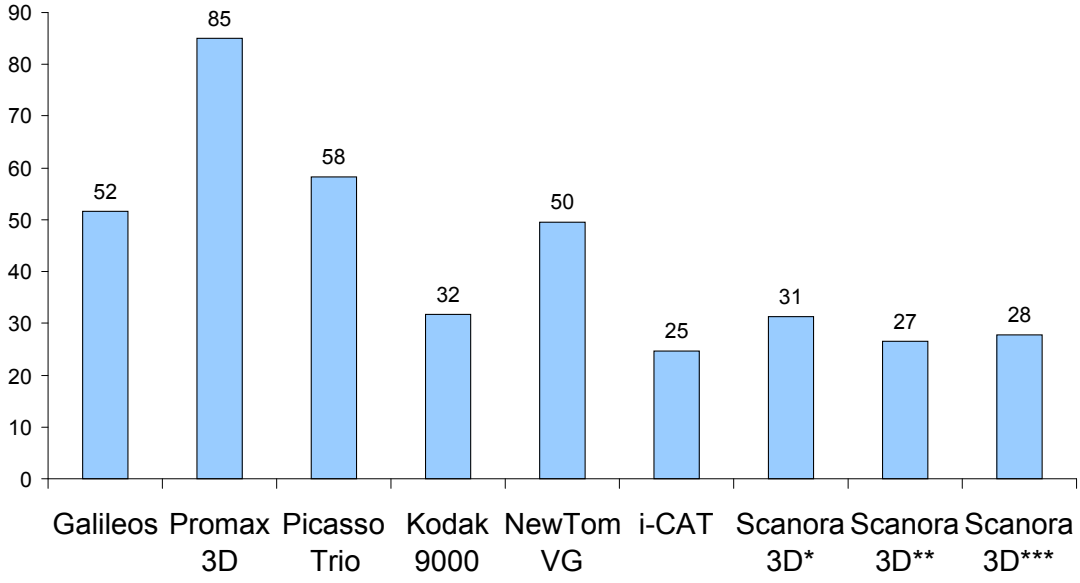

Figure 24. Adult effective dose (μSv)

***mandible, **maxilla, ***dento-alveolar**

Appendix 1 shows the exposure setting used for the paediatric dose measurements. Figure 25 shows the paediatric effective doses. Table 2 and Table 3 summarise the organ absorbed doses to the five radiosensitive organs for both paediatric phantoms. The effective doses range from 25 μSv to 81 μSv for a 10 year old and from 22 μSv to 63 μSv for an adolescent.

The maxilla imaging protocol of the Next Generation i-CAT unit and the 3D Accuitomo give the lowest effective doses for the two phantoms. The highest effective doses for both phantoms is observed for the NewTom VG unit due mainly to its fixed large FOV.

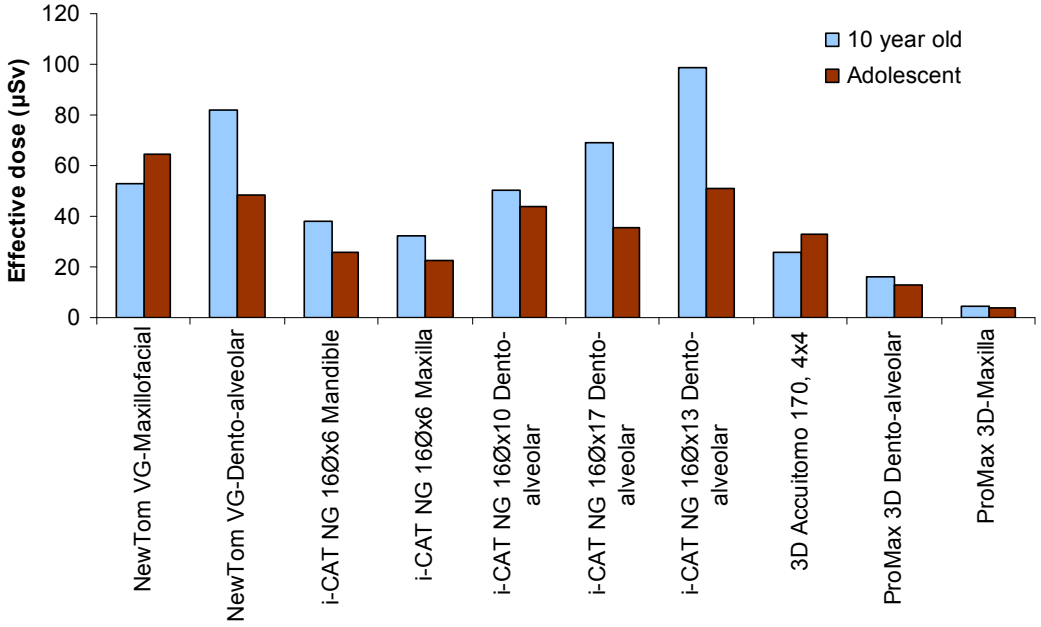

Figure 25. Paediatric effective doses (µSv)

Table 2 and Table 3 show that the bone marrow and skin absorbed doses are lower than the thyroid, salivary glands and brain absorbed doses. For the NewTom VG unit and for the maxillofacial protocol, the brain contributes the most to the effective dose for the 10 year old phantom while for the adolescent phantom the salivary glands contribute almost half of the effective dose. For the rest of the imaging protocols and units, the salivary glands contribute the most to the effective dose for the adolescent phantom while for the 10 year old phantom there is an almost equal contribution from the salivary glands and thyroid gland to the effective dose.

Table 2. Organ absorbed dose (mGy) for paediatric 10 year old phantom

Device	Bone Marrow	Skin	Thyroid	Salivary glands	Brain	Bone surface
NewTom VG Maxillofacial	0,165	0,088	0,197	0,708	1,584	0,165
NewTom VG Dento-alveolar	0,103	0,052	1,131	1,901	0,381	0,103
i-CAT 16Øx6 Mandible	0,045	0,030	0,380	1,584	0,077	0,045
i-CAT 16Øx6 Maxilla	0,086	0,036	0,190	1,021	0,285	0,086
i-CAT 16Øx10 Dento-alveolar	0,090	0,040	0,485	1,678	0,228	0,090
i-CAT 23Øx 17 Maxillofacial	0,091	0,044	1,007	1,175	0,499	0,091
i-CAT 16 Øx13 Maxillofacial	0,131	0,067	1,398	1,945	0,586	0,131
3D Accuitomo 170 4cmx4cm	0,024	0,021	0,217	1,333	0,034	0,024
Promax 3D Maxilla	0,012	0,015	0,028	0,170	0,023	0,012
Promax 3D Dento-alveolar	0,030	0,038	0,130	0,582	0,059	0,030

Table 3. Organ absorbed dose (mGy) for paediatric adolescent phantom

Device	Red Bone Marrow	Skin	Thyroid	Salivary glands	Brain	Bone surface
NewTom VG Maxillofacial	0,222	0,107	0,107	1,627	1,438	0,222
NewTom VG Dento-alveolar	0,106	0,063	0,297	1,970	0,228	0,106
i-CAT 16Øx6 Mandible	0,040	0,025	0,134	1,427	0,047	0,040
i-CAT 16Øx6 Maxilla	0,058	0,029	0,068	1,084	0,128	0,058
i-CAT 16Øx10 Dento-alveolar	0,123	0,052	0,194	1,813	0,167	0,123
i-CAT 23Øx17 Maxillofacial	0,038	0,033	0,179	2,009	0,042	0,038
i-CAT 16Øx13 Maxillofacial	0,084	0,043	0,222	1,143	0,364	0,084
3D Accuitomo 170 4cmx4cm	0,132	0,084	0,261	1,914	0,352	0,132
Promax 3D Maxilla	0,010	0,016	0,011	0,160	0,016	0,010
Promax 3D Dento-alveolar	0,032	0,017	0,042	0,566	0,091	0,032

4 Dose index proposals

4.1 Introduction

A wide number of dose measurements, using different CBCT devices, exposure protocols, phantoms and dosimeters have been presented in the previous section. Although it has been necessary to obtain a great amount of dosimetric information, it is important to summarize the information that is given by these measurements as much as possible. Therefore, before discussing the different possible approaches for the dose index, a summation will be given of the essential information that is acquired from the different measurements. Subsequently, the different approaches will be presented, along with an objective evaluation of their practical use.

4.2 Summary of results

Dose variability along Z-axis

As shown by ion chamber and TLD measurements in water, the dose remains relatively constant when measuring at different heights within the field of view. For large-field FOVs (but especially for wide cone angles), the difference in dose will be more pronounced. Similar to medical CT scanners with large beam widths, a decrease in the dose is observed outside the FOV along the z-axis. As in CT scanners, scatter tails have been observed for dental CBCTs which confirm the inadequacy of using a 100mm pencil chamber as a dosimetry tool.

Dose variability in XY plane due to positioning

In contrast with medical CT scanners, the dose distributions of dental CBCTs were found to be complicated. A clear difference was observed between central and off-axis positioning, which is more pronounced for small field of views. For full rotation exposures, the general pattern of the dose distribution remains the same, showing concentric (and left-right symmetrical) isodose curves around the isocentre. The peak of dose distribution shifts along with the position of the isocentre. An important aspect is that the dose values (for identical exposure settings) show a clear difference between central and off-axis exposure. If the field of view is closer to the periphery, the dose in this area will be higher compared to when it is positioned centrally. The proximity to the X-ray source for part of the CBCT's rotation is not compensated by a lower dose (due to more attenuation) coming from the opposite side. Another point, is that an exposure with a less than full rotation influences the shape of the dose distribution (as discussed below), but the difference between central and off-axis positioning remains the same, showing a shift in the distribution (but keeping the general shape and symmetry).

Dose variability in XY plane due to partial rotation

Again, a clear change in dose distribution is seen for those devices that use a partial rotation. A gradient is apparent, with the highest dose being found on the X-ray tube side of the phantom. For all the systems that we have examined, partial rotations have shown a left-right symmetry.

Dose variability in XY plane due to field of view size

A difference was seen between small FOVs of a few cm in diameter, and large volumes which (almost) cover the entire width of the phantom. For central positioning, the dose was highest in the central portion of the phantom for small FOVs, whereas for large FOVs the dose was higher at the periphery. Such a pattern was also observed for off-axis positioning.

Organ and effective dose measured using anthropomorphic phantoms

It was shown that the effective dose is affected by a number of parameters: the amount of exposure, the exposed volume, and the anatomical location of this volume. The large variation in effective dose between different CBCT devices and protocols is due to the absorbed dose at a few specific anatomical locations, most notably the thyroid and salivary glands. These findings affect the definition of a dose index, opening up the possibility for an anatomical dose index, which would be based on measurements performed at specific locations in a customized (head-like) phantom, and would provide an estimation of patient dose without a need for conversion. However, it is probably not feasible to put into routine practice but to estimate the amount and distribution of the radiation dose using a technical dose index, and apply conversion factors to obtain patient dose estimations.

In conclusions, for dental CBCT systems, dose distributions across the x-y plane and z-axis need to be assessed in order to derive a dose index that will a) characterise the volumetric dose distribution of dental CBCT scanners and b) correlate the dose index with the risk to the patient.

4.3 Dose index proposals

Three indices which characterise the dose distributions for dental CBCTs are proposed in this study. Two indices are measured in a standard PMMA phantom using a small-volume ion chamber at specific points. The third index is measured using a dose-area-product (DAP) meter, resulting in a single measurement of the incident dose multiplied by the beam area.

Index 1: measuring along diameter PMMA phantom

Using this method, measurements would be performed using an ion chamber or TLDs, along a diameter of the phantom (Figure 26). This would allow the measurement of an index for on axis and off-axis exposures, and full and partial dose distributions simply by rotating the phantom in such a way that

the isocentre of the x-ray beam lies on the measuring diameter as shown in Figure 26.

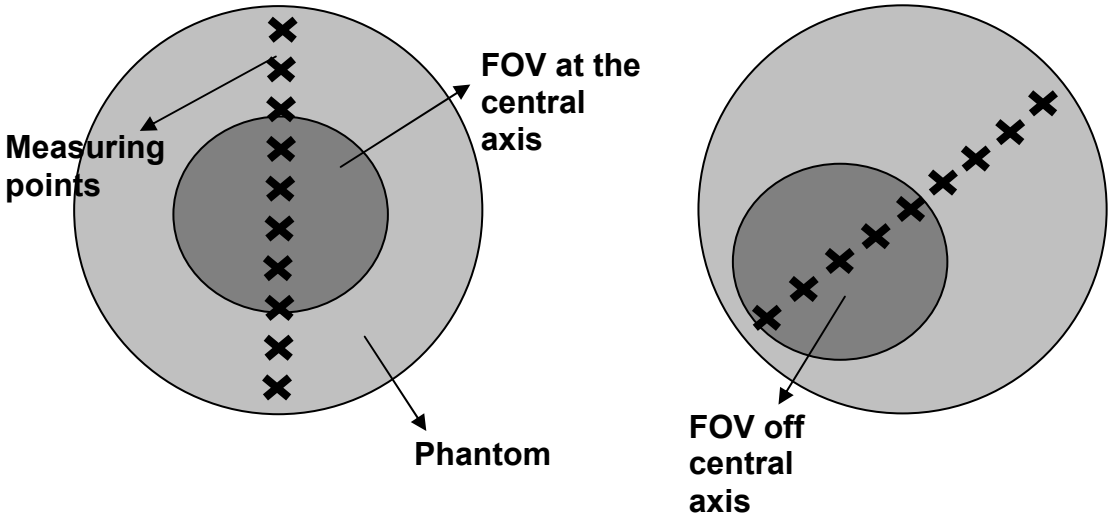

Figure 26. Measuring across the x-y plane of a customized PMMA phantom for axis and off-axis FOVs

The number of measurements along the diameter depends on the phantom design. If an ion chamber is used the holes should be drilled from the top of the phantom so that the central axis of the ion chamber would be perpendicular to the central axis of the x-ray beam. Such a design would eliminate any orientation inaccuracies for the ion chamber. A typical diameter of a small ion chamber is 2 cm so we recommend a 1 cm spacing with the first hole positioned 1 cm from the surface of the phantom for a 16cm diameter phantom. This would allow 6 measurements for a 16 diameter phantom. If TLDs are used as the preferred dosemeter, then a rod which would accommodate TLDs can be manufactured and inserted parallel at the central axis of the x-ray beam. The small size of the TLDs would allow a larger number of measurements along the measuring diameter but the accuracy of the TLD measuement is lower than the ion chamber.

Using a finite number of measurements along one line, a dose index could be defined as the average dose along this line:

$$DI1 = (Dx1 + ... + Dxn) / n$$

For a proper evaluation of the use of this index, the following need to be considered:

- Using this type of index, it is perfectly possible to use off-axis scanning (i.e. exposing the phantom as one would expose a patient), as long as left-right symmetry is kept. This would make the index more relevant for patient dose and risk estimation.

- The index is measured in one plane, and contains no information regarding the dose along the Z-axis, which is obviously important for a correlation to patient dose. Since the dose along the height of the FOV can be considered as homogeneous, it can be sufficient to add a conversion factor which is relative to the height of the FOV. This factor can be implemented into the index definition itself, or used solely for conversion to effective patient dose.
- Since the dose index is an average dose along a line, all information regarding dose distribution is lost. Different dose gradients can therefore result in an identical dose index value, and conversion to an effective dose would depend on positional factors, as well as the diameter of the FOV.

Measuring along a line would provide a good estimation of the amount of dose that is received throughout a head-sized phantom, and can be easily measured with a limited number of measurements and using an exposure geometry similar to that of a patient. Conversion to patient dose is not straightforward and requires information regarding the diameter and the height of the FOV and patient positioning protocols. Once the imaging protocols are established, factors can be defined to convert the dose index to effective doses for a range of positions and FOVs.

Index 2: measuring along peripheral circle and centre of PMMA phantom

This method resembles the existing CTDIw dose index which characterises dose distributions along the x-y plane for medical CT scanners. Absorbed doses are measured at the centre and at four points at the periphery of the phantom. Once the centre and average peripheral absorbed doses are determined, a weighting factor is applied to account for the non-uniform dose distribution across the x-y plane. The complicated dose distribution across the x-y plane for dental CBCTs could be measured using more than 4 peripheral points (Figure 27). Measurements can be done using a small ion chamber. Similar to dose index 1, holes should be drilled from the top for the insertion of the ion chamber.

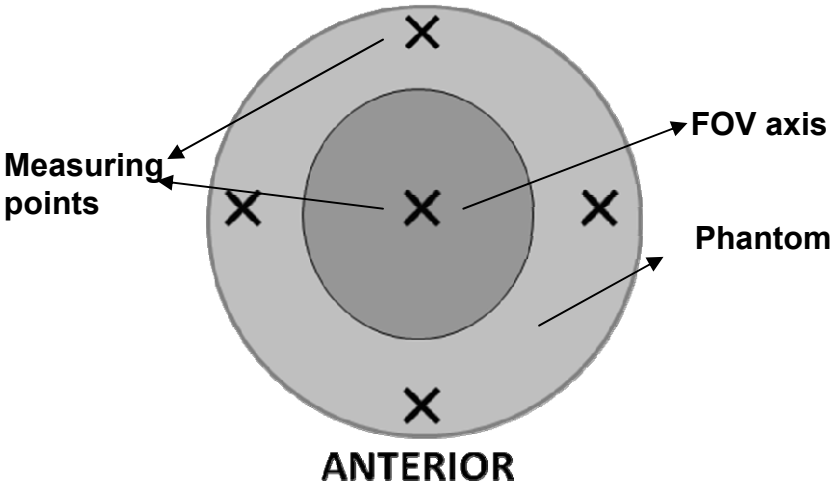

Figure 27. Measuring along the centre and periphery of a CTDI-like PMMA phantom. Crosses represent possible measurement locations. Four peripheral measuring points are shown, but more are possible

This dose index is appropriate for full rotation and central axis positioning only because for partial rotations and off-axis positioning there is a risk of missing dose gradients and maximum dose values if the measurement points are not within the FOV.

The index itself could be defined by calculating a weighted average of the central and peripheral measurements. However, the weighting factors that are used for the existing definition of CTDIw (1/3 central, 2/3 peripheral) are not appropriate for dental CBCTs because the dose distributions are more complicated than in conventional CT. For conventional CT, the weighting factors are derived assuming that the dose to the periphery is double the dose to the centre. For dental CBCTs with FOVs which cover the entire x-y plane, the dose distribution is almost constant so a weighting factor 1/2 would be appropriate. For small FOVs, the dose to the centre is higher than the periphery and the magnitude depends on the system and FOV which further complicates the definition of weighting factors.

This index, like the previous one, contains no information regarding Z-axis distribution, and the same considerations for comparing or converting it to an effective patient dose apply.

Many manufacturers of CBCT units quote CTDIw values measured at the centre and at four peripheral points in a PMMA phantom using a pencil chamber. In such cases, measuring the dose index could allow inter-comparison with the manufacturers' values but care will be needed in drawing any conclusions regarding the dose distributions of the systems.

To summarize, this index provides useful information for full rotational systems. However, for partial rotation and off axis positioning, this dose index

would not characterise fully the dose distribution. Correlation to patient dose is limited to full rotations and central positioning.

Index 3: the dose-area-product (DAP)

Using a DAP-meter is a straightforward and inexpensive method and highly popular among the medical physics community. This method is used in conventional dental and general radiography and it has been implemented into practice for dental CBCT, as many manufacturers have measured and reported DAP values for their systems and for a range of different protocols.

DAP provides information on the x-ray tube output and it depends on the exposure factors and field sizes. Since DAP is the product of the dose and the field size, it does not contain any exclusive information for both factors. For correlation to patient dose, the size of the FOV and positional factors will need to be taken into account, which may complicate interpretation of this index. However, with the increasing use of dose simulations such as the Monte Carlo method, it should be possible to obtain relationships between DAP and effective patient dose.

DAP meters are not designed to fit to CBCT tubes, and from our personal experience positioning the DAP-meter is not as easy as in general radiography and dental x-ray tubes.

Summarising, the DAP seems to be a useful dose index as measurement is relatively practical, it requires no customised phantom, and requires only a single measurement. The latter is of practical importance due to a lag time between subsequent CBCT exposures, which can be as long as a few minutes.

The indices into practice

Table 4 shows results based on the definition of the linear (index 1) and circular (index 2) dose indices, which are based on the TLD measurements described in the results section. For the circular dose index, the entire outside ring of TLD measurements was selected along with the central TLD measurement to provide an average dose.

The dose indices provide an estimation of the average dose throughout the entire phantom. However, to allow a correlation to an effective dose, there is a location parameter needed which shows how the dose is distributed spatially. For index 1, the standard deviation provides information regarding dose uniformity. The existence and location of the inhomogeneity along the measuring line could be determined by plotting the doses. However, to assess the inhomogeneity further a more complex calculation is needed based on individual measurements or groups of adjacent measurements. For index 2, the difference between the standard deviation of the entire group of measurements and those of the periphery provides some information regarding the homogeneity, as well as the spatial distribution. However, as

dor dose index 1, a more spatially dependent calculation is required to determine the peak and gradient of the dose distribution.

Table 4. Dose index estimations based on TLD measurements. Average and standard deviations for both indices' measurement locations are shown, as well as the standard deviation of the peripheral measurements for the second index.

			Index 1		Index 2		
Device	Rotation	Positioning	Avg dose	St.dev	Avg dose	St.dev	St.dev peripheral
GALILEOS	half	off-axis	2,153	0,597	2,545	0,842	0,858
SCANORA 3D	full	off-axis	1,495	0,173	1,545	0,239	0,244
Illuma	full	central	2,340	0,133	2,303	0,137	0,140
Illuma	full	off-axis	0,793	0,200	0,835	0,243	0,248
NewTom VG	full	central	2,358	0,103	2,522	0,082	0,071
NewTom VG	full	off-axis	1,828	0,131	1,851	0,240	0,247
3D Accuitomo 170	full	central	2,510	0,327	2,214	0,309	0,149
3D Accuitomo 170	full	off-axis	2,102	0,954	2,203	0,733	0,754
3D Accuitomo 170	full	central	4,285	0,552	3,627	0,420	0,183
3D Accuitomo 170	full	central	4,892	0,566	4,616	0,322	0,224
3D Accuitomo 170	full	central	6,432	0,239	6,246	0,181	0,161
3D Accuitomo 170	full	central	7,437	0,440	7,370	0,257	0,238
3D Accuitomo 170	half	central	4,079	1,877	3,608	2,044	2,113
i-CAT NG	full	central	1,429	0,120	1,482	0,092	0,090
i-CAT NG	full	off-axis	1,302	0,200	1,403	0,215	0,222
i-CAT NG	full	central	1,345	0,221	1,216	0,155	0,147
i-CAT NG	half	central	0,703	0,302	0,676	0,335	0,348
i-CAT NG	full	off-axis	1,315	0,324	1,226	0,358	0,371
ProMax 3D	half	central	0,867	0,344	0,791	0,358	0,369
ProMax 3D	half	central	0,853	0,391	0,788	0,381	0,394
ProMax 3D	half	off-axis	0,858	0,129	0,870	0,182	0,188

Figure 28 shows that there is a high degree of linearity seen, and that the actual values are similar as well. The difference between the indices ranges from -18% to +15%, even though most (all but four) differences are within a -10% to +10% interval.

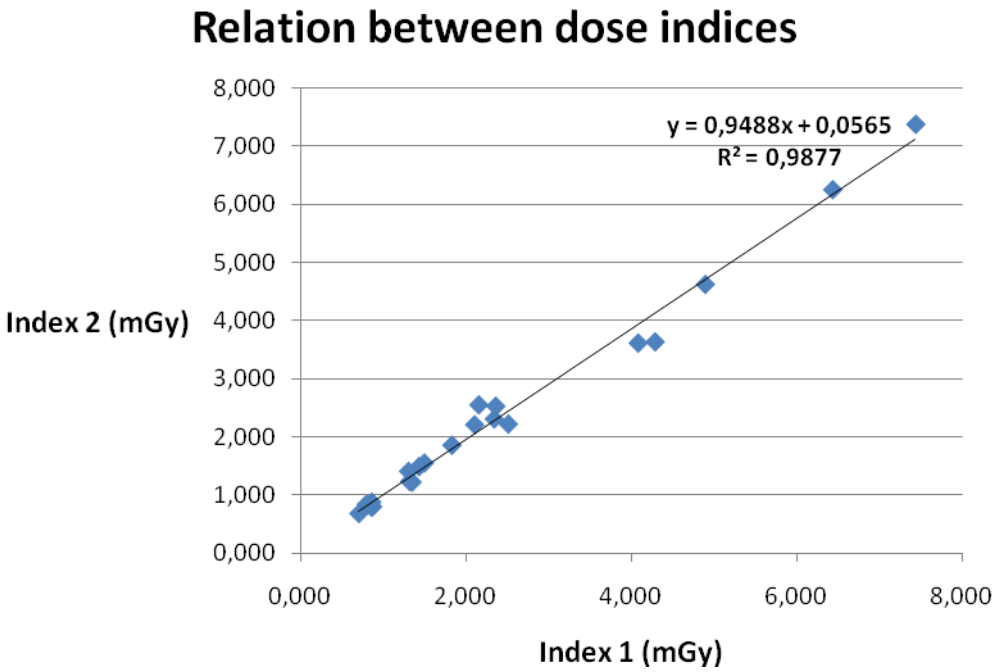

Figure 28. Correlation plot for two proposed indices, showing linear correlation coefficient (R^2)

Figure 29 shows the dose distribution (used for index 1) along a measuring line for four distinct types of CBCT exposures. There is a uniform distribution for the NewTom VG because the FOV covers the entire x-y plane. For the 3D Accuitomo 170 (FOV=6cmØ x 6cm height), there is an increase followed by a plateau at the central region of the phantom and then there is a decrease towards the back edge of the phantom. For the off-axis i-CAT NG (8cmØ), the isocentre was positioned towards the back edge of the phantom to simulate the patient positioning, and it may be seen that the dose starts from a maximum value at the back of the phantom and decreases towards the front of the phantom. Finally, the i-CAT NG half rotation shows a similar pattern to the i-CAT off axis. The back side of the phantom is irradiated during a half rotation which is depicted on the graph. The graph shows that measuring along a line gives a very good estimate of the dose distribution.

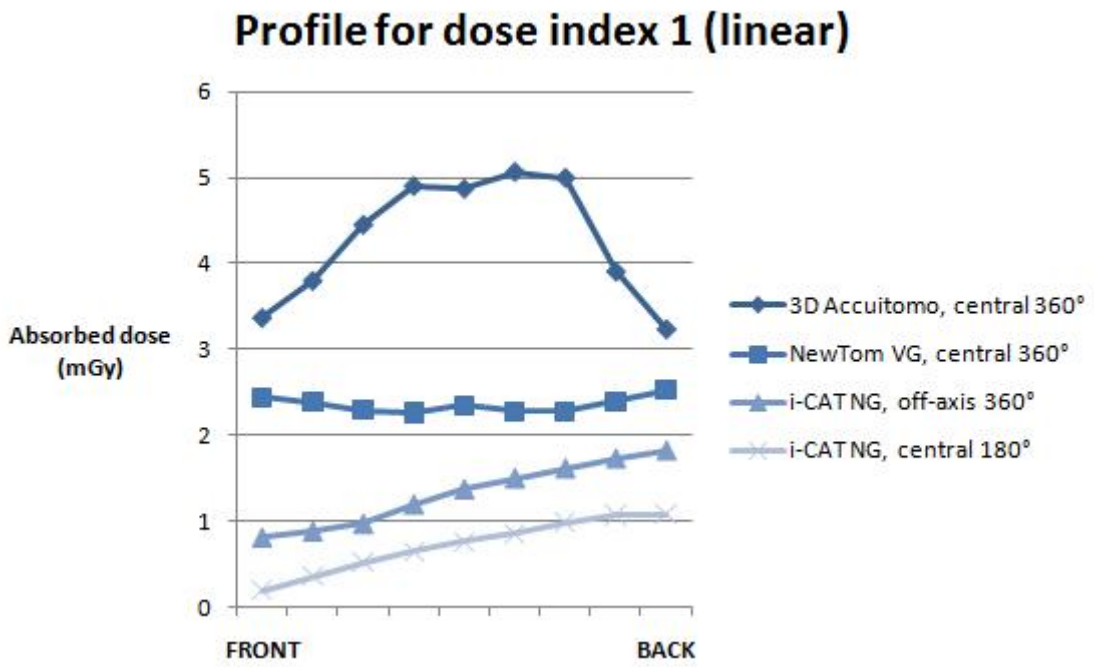

Figure 29. Dose profiles of dose index 1 based on TLD measurements

The DAP measurements have been presented and discussed above. Their implementation into practice is clearly understood, although they possess no spatial information whatsoever, and any correlation with an effective dose will have to be calculated based on a number of parameters, most importantly the size and position of the FOV.

5. Conclusions

In this report, the results of different types of measurements are presented which aid in the development of a dose index, by either determining the dose distribution throughout homogeneous phantoms or estimating the absorbed organ dose within anthropomorphic phantoms.

From TLD and ion chamber measurements in cylindrical water and PMMA phantoms, the shape and extent of the scatter tail along the z-axis was determined. It was shown that the dose drops significantly when moving outside the primary beam. It was also shown that the dose can be distributed asymmetrically when the isocentre is not positioned in the centre of the cylinder, or when the CBCT device uses an exposure of less than 360°.

From TLD measurements using adult and paediatric phantoms, it was shown that the effective dose and the individual organ absorbed doses can vary depending on the FOV size and positioning, and the amount and energy of exposure. It was also clear that the effective dose from a dental CBCT exposure is mainly defined by the absorbed dose of the salivary glands and thyroid gland, and the bone marrow to a lesser extent. These findings suggest that the risk to the patient may be characterized by the absorbed dose at a few anatomical positions.

Different dose indices are proposed, each estimating the amount of exposure in their own way. Two indices require measurements performed by a small-volume ion chamber at pre-defined locations in a head-sized PMMA phantom. The third index is the DAP which has been applied for other X-ray modalities, and recently has been introduced for dental CBCT as well.

Further investigations should be made to assess the validity and practicality of a) the dose indices using a small ion chamber and a suitable PMMA phantom and b) the use of DAP. Furthermore, the relationship between the dose indices and the effective dose would be investigated using Monte Carlo simulations and mathematical modeling (SedentexCT WP 2.4).

References

Boone JM, Cooper VN 3rd, Nemzek WR, McGahan JP, Seibert JA. Monte Carlo assessment of computed tomography dose to tissue adjacent to the scanned volume. Med Phys. 2000 Oct;27(10):2393-407.

Brenner DJ. It is time to retire the computed tomography dose index (CTDI) for CT quality assurance and dose optimization. For the proposition. Med Phys. 2006 May;33(5):1189-90.

Dixon RL. A new look at CT dose measurement: beyond CTDI. Med Phys. 2003 Jun;30(6):1272-80.

Fearon T. CT dose parameters and their limitations. Pediatr Radiol. 2002 Apr;32(4):246-9.

Huda W, Sandison GA. Estimation of mean organ doses in diagnostic radiology from Rando phantom measurements. Health Phys 1984;47:463-467.

Jessen KA, Shrimpton PC, Geleijns J, Panzer W, Tosi G. Dosimetry for optimisation of patient protection in computed tomography. Appl Radiat Isot. 1999 Jan;50(1):165-72.

Lofthag-Hansen S, Thilander-Klang A, Ekestubbe A, Helmrot E, Gröndahl K. Calculating effective dose on a cone beam computed tomography device: 3D Accuitomo and 3D Accuitomo FPD. Dentomaxillofac Radiol. 2008 Feb;37(2):72-9.

Loubele M, Jacobs R, Maes F, et al. Radiation dose vs. image quality for low-dose CT protocols of the head for maxillofacial surgery and oral implant planning. Radiat Prot Dosimetry 2006; 117:211-6.

Mori S, Endo M, Nishizawa K, *et al*. Enlarged longitudinal dose profiles in cone-beam CT and the need for modified dosimetry. Med Phys. 2005 Apr;32(4):1061-9.

Nakonechny KD, Fallone BG, Rathee S. Novel methods of measuring single scan dose profiles and cumulative dose in CT. Med Phys. 2005 Jan;32(1):98-109.

Perisinakis K, Damilakis J, Tzedakis A, Papadakis A, Theocharopoulos N, Gourtsoyiannis N. Determination of the weighted CT dose index in modern multi-detector CT scanners. Phys Med Biol. 2007 Nov 7;52(21):6485-95.

Appendix 1 CBCT exposure settings

Exposure factors and clinical indication used for water and PMMA phantom measurements

Device	Rotation	Positioning	kVp	mAs	FOV size (cm)
Ion chamber water					
SCANORA 3D	full	central	85	30	10x7.5
TLD water x-z plane					
SCANORA 3D	full	central	85	30	10x7.5
SCANORA 3D	full	off-axis	85	36	6x6
3D Accuitomo XYZ	full	off-axis	80	70	4x3
TLD water & PMMA x-y plane					
GALILEOS	half	off-axis	85	28	15x15
SCANORA 3D	full	off-axis	85	30	100x75
Iluma	full	central	120	High	Large
Iluma	full	off-axis	120	Low	Large
NewTom VG	full	central	110	9.58	23x23
NewTom VG	full	off-axis	110	6.12	23x23
3D Accuitomo 170	full	central	90	87,5	4x4
3D Accuitomo 170	full	off-axis	90	87,5	4x4
3D Accuitomo 170	full	central	90	87,5	6x6
3D Accuitomo 170	full	central	90	87,5	8x8
3D Accuitomo 170	full	central	90	87,5	14x5
3D Accuitomo 170	full	central	90	87,5	14x10
3D Accuitomo 170	half	central	90	87,5	10x10
i-CAT NG	full	central	120	18.54	16x6
i-CAT NG	full	off-axis	120	18.54	16x6
i-CAT NG	full	central	120	18.54	8x8
i-CAT NG	half	central	120	18.54	8x8
i-CAT NG	full	off-axis	120	18.54	8x8
ProMax 3D	half	central	84	17.1	8x5
ProMax 3D	half	central	84	17.1	8x8
ProMax 3D	half	off-axis	84	17.1	8x5

Exposure factors and clinical indication used for the adult anthropomorphic phantom measurements

	kVp	mAs	Voxel size (mm)	Field of View (cm)	Clinical Indication
Galileos	85	28	0.3	15	Dento-alveolar
Promax 3D	84	114	0.16	8	Mandible + half maxilla
Picasso Trio	85	53	0.2	12 Ø x 7	Mandible
Kodak 9000	70	105	0.076	5 Ø x 3.7	Mandible Front
NewTom VG	110	10	0.3	15 Ø	Dento-alveolar
i-CAT Next Generation	120	19	0.4	16 Ø x 6	Mandible
Scanora 3D	85	30	0.2	10 Ø x 7.5	Mandible, Maxilla, Dento-alveolar

Exposure factors and clinical indication used for the paediatric anthropomorphic phantom measurements

	NewTom VG		**Planmeca Promax 3D**		**Next Generation i-CAT (all protocols)**	**3D Accuitomo 170**
	10 year	Adolescent	10 year	Adolescent	10 year & Adolescent	10 year & Adolescent
kVp	110	110	84	84	120	90
mA	2.5	2			5	5
mAs	8.2 (D) 15.8 (M)	4.8 (D) 11.7 (M)	16.9 (Max) 19.9 (D)	4.5(Max) 17.1(D)	18.5	
Scan time						17.5
FOV (cm)	15Ø	15Ø	8Øx5(Max) 8Øx8(D)	8Øx5(Max) 8Øx8(D)	16Øx6(H) 16Øx10(H) 16Øx13(H) 23Øx17(H)	4x4
Voxel size (mm)	0.3	0.3	0.16	0.16	0.4	
Examination Protocol	Dento-alveolar M	Dento-alveolar M	Maxilla Dento-alveolar	Maxilla Dento-alveolar	Mandible Maxilla Dento-alveolar Max	

EUROPEAN COMMISSION
European Research Area